

**Modelling of
subduction interplate
dynamics**

D. Arcay

Dynamics of interplate domain in subduction zones: influence of rheological parameters and subducting plate age

D. Arcay

Géosciences Montpellier, University Montpellier 2, CNRS, UMR 5243, Montpellier, France

Received: 30 June 2012 – Accepted: 6 July 2012 – Published: 20 July 2012

Correspondence to: D. Arcay (diane.arcay@gm.univ-montp2.fr)

Published by Copernicus Publications on behalf of the European Geosciences Union.

Title Page

Abstract

Introduction

Conclusions

References

Tables

Figures



Back

Close

Full Screen / Esc

Printer-friendly Version

Interactive Discussion



Abstract

The properties of the subduction interplate domain are likely to affect not only the seismic potential of the subduction area but also the overall subduction process, as it influences its viability. Numerical simulations are performed to model the long-term equilibrium state of the subduction interplate when the diving lithosphere interacts with both the overriding plate and the surrounding convective mantle. The thermomechanical model combines a non-Newtonian viscous rheology and a pseudo-brittle rheology. Rock strength here depends on depth, temperature and stress, for both oceanic crust and mantle rocks. I study the evolution through time of, on one hand, the kinematic decoupling depth, z_{dec} and, on the other hand, of the brittle-ductile transition (BDT) depth, z_{BDT} , simulated along the subduction interplate. The results reveal that z_{BDT} mainly depends on the friction coefficient characterising the interplate channel and on the viscosity at the lithosphere-asthenosphere boundary. The influence of the weak material activation energy is of second order but not negligible. z_{BDT} becomes dependent on the ductile strength increase with depth (activation volume) if the BDT occurs at the interplate decoupling depth. Regarding the interplate decoupling depth, it is basically a function of (1) mantle viscosity at asthenospheric wedge tip, (2) difference in mantle and interplate activation energy, and (3) activation volume. Specific conditions yielding $z_{\text{BDT}} = z_{\text{dec}}$ are discussed. I then present how the subducting lithosphere age affects the brittle-ductile transition depth and the kinematic decoupling depth in this model. Simulations show that a rheological model in which the respective activation energies of mantle and interplate material are too close impedes strain localization during incipient subduction of a young (20 Myr old) and soft lithosphere under a thick upper plate. Finally, both the BDT depth and the decoupling depth are a function of the subducting plate age, but are not influenced in the same fashion: cool and old subducting plates deepen the BDT but shallow the interplate decoupling depth. Even if BDT and kinematic decoupling are intrinsically related to different mechanisms of deformation, this work shows that they are able to interact closely.

Modelling of subduction interplate dynamics

D. Arcay

Title Page

Abstract

Introduction

Conclusions

References

Tables

Figures

◀

▶

◀

▶

Back

Close

Full Screen / Esc

Printer-friendly Version

Interactive Discussion



complete viscous mechanical coupling between plates takes place and the lower part of the fore-arc mantle is ablated, ending to an extreme heating at shallow depth (e.g. Eberle et al., 2002). Several methods have been explored to decouple kinematically the two converging plates. A first set is based on kinematic assumptions, such as complete free slip along the boundary (Furukawa, 1993), rigid and motionless fore-arc lithosphere (Peacock and Hyndman, 1999; van Keken et al., 2002), or simulation of a progressive kinematic coupling between the upper lithosphere base and the subducting slab (Kneller et al., 2005, 2007; Syracuse et al., 2010). Another approach aims at simulating low strength/low shear along the boundary, by assigning low viscosity to the interface nodes (Billen and Gurnis, 2001; Kelemen et al., 2003; Wada et al., 2008; Wada and Wang, 2009), limiting shear stress (Zhong and Gurnis, 1995; van Hunen et al., 2002), or impeding fore-arc deformation if predicted to occur in the brittle domain, itself delimited by a predetermined temperature (Conder, 2005; Syracuse et al., 2010). Thermo-kinematic models with a prescribed interplate mechanics are useful to test specific assumptions suggested by observations, such as partial melting domain extent and/or geometry of the cold fore-arc nose, before returning back to observations to evaluate the simulated picture, because subduction geometry is then easily adjusted to fit the observed one. However, one part of the involved physics regulating the interplate equilibrium cannot be resolved and demands a dynamic modelling in which temperature, flow, and stress evolves freely and consistently as a function of their own interactions. This is the main purpose motivating this paper.

Numerical models are performed to study the equilibrium state of the subduction interplate when the diving lithosphere interacts with both the overriding plate and the surrounding convective mantle, after 650–900 km of subduction, i.e., when the subduction transient state ends. The decoupling interface geometry is not fixed and its properties are not assigned, as both evolve as a function of advection within the interplate of weak crustal material. Rock strength here depends on depth, temperature and stress, for both mantle rocks and the weak crust filling the interplate domain. The thermo-mechanical model combines a non-Newtonian viscous rheology and a pseudo-brittle

SED

4, 943–992, 2012

Modelling of subduction interplate dynamics

D. Arcay

Title Page

Abstract

Introduction

Conclusions

References

Tables

Figures

◀

▶

◀

▶

Back

Close

Full Screen / Esc

Printer-friendly Version

Interactive Discussion



rheology. By combining these two mechanical behaviours, one is then able to study how the limit of the brittle realm along the subduction plane, on the one hand, and the down-dip extent of kinematic decoupling between the two converging lithospheres, on the other hand, stabilise through time and possibly interact, as a function of (1) rheological parameters and (2) subduction parameters (convergence rate, subducting lithosphere and upper plate structures, asthenosphere flows). The paper focuses on the influence of the subducting lithosphere age.

1.2 Depth of interplate kinematic decoupling vs. depth of brittle-ductile transition

From a kinematic approach, the tangential displacement of the overlying lithosphere and the subducting slab are decoupled on both sides of the interplate interface. Below the interplate decoupling depth, mantle rocks above the subducting slab are passively dragged down by the latter. The transition depth between decoupled motions above and coupled displacements below is labelled the “interplate decoupling depth” (Furukawa, 1993). Advection of warm asthenospheric rocks occurs into the wedge to replace the mantle dragged down along the slab by viscous coupling across the slab top (labelled “corner flow”, Fig. 1a). This rising return flow is mainly passive. As a result, a high temperature increase occurs across the slab top in the vicinity of the interplate decoupling depth, resulting in a drastic mantle viscosity decrease if the rheology is non-Newtonian and temperature-dependent (Andrews and Sleep, 1974; Honda, 1985), and entails a corner flow focussing at the interplate decoupling base. Moreover, focused high strain rates, confined in the decoupling interface until its base, jumps there away from the slab surface and reaches the asthenospheric wedge over a relatively narrow interval where thermal gradients are very high (Fig. 1a). Therefore, the interplate decoupling depth results from a thermomechanical equilibrium, probably depending on the asthenosphere/interplate material strength contrast, but also on subduction characteristics, such as convergence rate, that governs interplate strain rates and flow velocities within the mantle wedge.

Modelling of subduction interplate dynamics

D. Arcay

Title Page

Abstract

Introduction

Conclusions

References

Tables

Figures



Back

Close

Full Screen / Esc

Printer-friendly Version

Interactive Discussion



plate ~ 100 km thick, by varying brittle strength but also the non-Newtonian strength. I then lean on the derived conclusions to explain why the subduction of a young lithosphere may be sustainable or not, depending on the modelled rheology. The influence of the convergence rate on z_{dec} has been already extensively studied elsewhere and is not investigated here.

2 Model set-up

A thermochemical code of convection (Christensen and Yuen, 1984; Christensen, 1992) is used to model subduction. It solves the momentum, energy, and mass conservation equations. Rocks are assumed to be incompressible, except for the thermal buoyancy term in the momentum equation, and for the adiabatic heating term (Table 1) in the energy equation (extended Boussinesq approximation). Shear heating (i.e., viscous and frictional dissipations) and uniform heat production are also included in the heat conservation equation. Indeed, shear heating has been shown to help significantly strain localisation and weak strength inside the subduction interface by sustaining high temperature (e.g. Doin and Henry, 2001; Faccenda et al., 2008). The simulation box is 2220 km wide and 555 km high (Fig. 2). Composition (either mantle or weak crust) is tracked by two types of tracer that have different densities and rheological properties. Buoyancy depends on temperature, through the thermal expansion coefficient, and composition (crust/mantle). Compositional tracers are advected with the velocity field (van Keken et al., 1997).

2.1 Mechanical boundary conditions and subduction modelling

Subduction is simulated by applying a constant convergence rate, $v_{\text{sub}} = 6.5 \text{ cm yr}^{-1}$ on-top of the incoming lithosphere, on a 832 km wide and 16 km deep segment (Fig. 2). The diving plate then evolves freely within the trench area. The upper lithosphere is 100 km thick and is here assumed to be simply made of mantle rocks. The incoming

SED

4, 943–992, 2012

Modelling of subduction interplate dynamics

D. Arcay

Title Page

Abstract

Introduction

Conclusions

References

Tables

Figures

◀

▶

◀

▶

Back

Close

Full Screen / Esc

Printer-friendly Version

Interactive Discussion



Modelling of subduction interplate dynamics

D. Arcay

Title Page

Abstract

Introduction

Conclusions

References

Tables

Figures



Back

Close

Full Screen / Esc

Printer-friendly Version

Interactive Discussion



plate is covered by a 7 km thick layer of “crust” material much weaker than the underlying mantle. At simulation start, an initial 30° dipping interplate plate made of weak crust material is imposed from the surface to 55 km depth, at the middle of the box. The trench is hence initially located 1110 km away from the left-hand side of the box.

5 Strain localisation along the interplate boundary during convergence basically relies on the strength contrast between mantle rocks, composing the upper lithosphere but also the remaining part of the subducting plate. Deformation localisation along the convergence boundary is then a function not only of the specific mechanical properties of the modelled mantle and crust, but also on the interplate geotherm, or, more precisely, on
10 the difference between interplate and upper plate geotherms. If the thermo-mechanical conditions are such that the weak crustal material is able to localise deformation, the subducting mantle lithosphere bends, and the weak material flows at the subducting plate surface to continuously filled the initial interplate channel. Subduction in this case is successfully initiated and is sustained by the constant convergence rate.

15 The lower boundary is open to prevent the slab deformation that would occur when the slab encounters the box base. However, a vertical resistance against flow is modelled in some simulations to help the convective mantle, if not strong enough, to compensate the subducting slab weight. If k is the wavenumber of a harmonic vertical flow field, the resistance to vertical flows applied at box bottom, R_b , writes as: $R_b = \nu \times k$,
20 where ν is the viscosity of the material that would underlie the open lower boundary. The boundary condition at box bottom is: $\sigma_{zz} - 2R_b v_z = 0$, where σ_{zz} is the non-hydrostatic vertical stress and v_z is the vertical velocity (Ribe and Christensen, 1994). By setting the reference strain rate in the model, $\dot{\epsilon}_{ref}$, to 10^{-14} s^{-1} , and the subduction velocity, v_{sub} , to 6.5 cm yr^{-1} , the vertical scale length of deformation is: $L = v_{sub} / \dot{\epsilon}_{ref}$,
25 that defines here the main wavelength of deformation, k^{-1} . ν is set to either the normal viscosity at box bottom, ν_{BB}^* : $\nu_{BB}^* = 1$ in $\nu = \nu_{BB} \times \nu_{BB}^*$ (no viscosity jump across the lower boundary, simulations S10 and S12 for instance in Table 2), or 10 times the viscosity at 555 km depth ($\nu_{BB}^* = 10$, e.g. simulations S12 and S13, Table 2). Other mechanical boundary conditions are presented in Fig. 2.

2.2 Thermal boundary conditions – modelling subduction of a constant age-at-trench lithosphere

The whole convective box is heated by a uniform radiogenic source (Table 1). Along the surface, the temperature is set to 0 °C, whereas across all other boundaries are insulating. At subduction initiation, the upper lithosphere thermal structure is that of an old (≈ 100 Myr) and cold lithosphere, at equilibrium with the underlying convective mantle, thence stable. The same thermal state is applied for the incoming plate in models of 100 Myr-old lithosphere subduction (Sect. 3). This thermal structure insures constant equilibrium between cooling from above and heating from below by asthenosphere convective flows, which prevent any plate thermal thickening during subduction. The simulation box thermal structure is the result of a preliminary run in the same conditions as described above, but without convergence velocity. The lithosphere has finally a homogeneous 100 km thickness (Fig. 2a), with basal small perturbations resulting from small-scale convection. A pseudo-ridge is imposed at the incoming lithosphere extremity, and simulates the plate conductive cooling from 0 Ma to a chosen lithosphere age, A_{lith} , on a 400 km width (Fig. 2). The structure of this pseudo-ridge is constantly sustained as a boundary condition, and is used to re-generate the incoming lithosphere while it is consumed by the subduction process. An overlying layer of 7 km weak crustal material is also constantly maintained on the surface of the newly formed lithosphere. As imposed by the assigned boundary conditions, a segment of lithosphere with age A_{lith} , is located 710 km away from the trench and thus undergoes an ageing of ≈ 11 Myr during its route to the subduction trench at a speed of 6.5 cm yr^{-1} . As a consequence, the value of A_{lith} is set to 90 Myr to account for the newly formed lithosphere cooling and thickening and finally to model a subducting lithosphere of constant age.

The thermal thickness of a 20 Myr old-subducting lithosphere, defined by the 1200 °C isotherm depth, should be close to 52 km according to the half-space cooling model (Turcotte and Schubert, 1982). However, this thickness results in a predicted surface heat flux of 69 mWm^{-2} for the thermal conductivity here assumed (Table 1),

SED

4, 943–992, 2012

Modelling of subduction interplate dynamics

D. Arcay

Title Page

Abstract

Introduction

Conclusions

References

Tables

Figures

◀

▶

◀

▶

Back

Close

Full Screen / Esc

Printer-friendly Version

Interactive Discussion



Modelling of subduction interplate dynamics

D. Arcay

Title Page

Abstract

Introduction

Conclusions

References

Tables

Figures

◀

▶

◀

▶

Back

Close

Full Screen / Esc

Printer-friendly Version

Interactive Discussion



whereas surface heat flux estimate of oceanic basin floor indicate a value of rather $\approx 112 \text{ mW m}^{-2}$ for a 20 Myr old oceanic lithosphere (Doin and Fleitout, 1996). This high heat flux would imply a very hot lithosphere only 31 km thick. A compromise temperature gradient of 34.6°C/km is imposed from the surface to the lithosphere base (39 km depth) to mimic a 20 Myr old plate. A_{lith} is then adjusted to 10 Myr to maintain a roughly constant lithospheric age of 20 Myr at the trench. Note that the thermal structure of the interplate area is a bit cooled at subduction onset for hot incoming plates to help strain localisation. Isotherms of the incoming lithosphere are curved to be parallel to the subduction plane, which enhances the strength of the first subducting lithospheric mantle segment and favor deformation localisation within the weak plane (Fig. 2b).

2.3 Rheology

2.3.1 Rheological model

The rheological model combines a pseudo-brittle rheology, with a yield stress increasing with depth to a non-Newtonian creep rheology. An effective viscosity, ν_{eff} , is defined through the relationship: $\tau = \nu_{\text{eff}} \dot{\epsilon}$, where τ and $\dot{\epsilon}$ are the second invariants of the stress and strain rate tensors, respectively. The effective viscosity is given by the inverse average between a brittle-plastic term, ν_{b} , and the non-Newtonian viscosity strength, ν_{v} : $\nu_{\text{eff}}^{-1} = \nu_{\text{b}}^{-1} + \nu_{\text{v}}^{-1}$, assuming that the total deformation is the sum of brittle and ductile strains.

The pseudo-brittle rheology is modelled through a yield stress, τ_{y} , increasing with depth, z : $\tau_{\text{y}} = \tau_0 + \gamma_{\text{c}}(C)\rho g z$, where τ_0 is the cohesive strength at the surface and γ_{c} is a coefficient depending here on composition. This coefficient is related to the friction coefficient, f_{s} , through the relationship (Turcotte and Schubert, 1982): $\gamma_{\text{c}} = 2f_{\text{s}}(1 - \rho_{\text{w}}/\rho)/((1 + f_{\text{s}}^2)^{1/2} - f_{\text{s}})$, where ρ_{w} is the water density. The effective plastic vis-

cosity, ν_b , is given by:

$$\nu_b = \tau_y \frac{\dot{\epsilon}^{\frac{1}{n_p}-1}}{\dot{\epsilon}_{\text{ref}}^{\frac{1}{n_p}}} \quad (1)$$

where $\dot{\epsilon}_{\text{ref}}$ is a reference strain rate and n_p is a large stress coefficient (Table 1). In the plastic domain, very large strain rates are simulated as soon as stress exceeds the yield stress. The non-Newtonian rock viscosity, ν_v , writes as:

$$\nu_v = A_0 \exp\left(\frac{E_a(C) + V_a a_a \rho g z}{nRT}\right) \dot{\epsilon}^{\frac{1}{n}-1} \quad (2)$$

where T is temperature in Kelvin, A_0 is the pre-exponential constant, E_a is the activation energy, depending on composition, V_a is the activation volume, n is an exponent different from 1, and R is the gas constant (Table 1). The choice of a non-Newtonian rheology in the creep deformation model favors the development of a self-sustaining low localisation of deformation within area of high strain-rate and low strength and facilitates subduction initiation (Billen and Gurnis, 2005).

In two simulations (S13f14 and S13f14b, Table 2), a local viscosity decrease is modeled in the mantle wedge area by simulating (1) slab dehydration related to destabilisation of oceanic crust hydrous minerals and deserpentinisation of the underlying subducting cold mantle, (2) vertical migration of expelled fluids and subsequent water-saturation of the overlying asthenospheric rocks in the hydrated mantle wedge area, and (3) hydrous strength weakening for hydrated mantle rocks. The model of slab dehydration prediction-mantle wedge hydration in the absence of slab melting based on accurate $P - T$ phase diagrams was extensively described in Arcay et al. (2005, 2006). I do not want to go into the details of the modeling, since the objective in this paper is to use it as a way to simulate a viscosity decrease only in the vicinity of the mantle wedge tip where the subduction interface ends. In a nutshell, the dehydration-hydration geometry is basically a function of the diving lithosphere thermal state. For a 6.5 cm yr^{-1}

Modelling of subduction interplate dynamics

D. Arcay

Title Page

Abstract

Introduction

Conclusions

References

Tables

Figures

◀

▶

◀

▶

Back

Close

Full Screen / Esc

Printer-friendly Version

Interactive Discussion



convergence rate and a 100 Myr old plate, the hydrated area width in the mantle wedge equals at maximum 133 km, 6.5 Myr after subduction initiation, and decreases to the steady value of 84 km at 15 Myr, because the subducting dip angle increases while slab pull develops. I choose to reduce for water-saturated rocks the pre-exponential constant in Eq. (2) to $A_0/14$, which results in a hydrous strength reduction of $14^{3/2} \sim 52$ (Table 2) if effective non-Newtonian viscosity has to be expressed rather as a function of the energy dissipation rate, $(\sigma\dot{\epsilon})$, than strain rate, $\dot{\epsilon}$ (Christensen, 1984; Dumoulin et al., 1999).

2.3.2 Choice of rheological parameter sets investigated in this paper

The goal is to investigate the interplay between brittle and ductile rheologies along the subduction interface. As brittle deformation is basically controlled by the friction coefficient, the unique parameter that will be tested is the weak layer frictional coefficient, γ_c , keeping constant the cohesive strength at the surface, C_0 , the exponent n_p in equation 1 and the reference strain rate, $\dot{\epsilon}_{ref}$. To simplify, the mantle friction coefficient, γ_m , will also remain set to 1.6 (Table 1).

In this paper, creep behaviour is a function of temperature, pressure, strain rate, and composition (mantle/weak layer). The temperature-dependence in viscosity is controlled by the activation energy whereas the pressure-dependence increases with the activation volume, V_a (Eq. 2). The respective effects of V_a , weak crust and mantle activation energies, E_a^c and E_a^m , will all be tested. One may note that activation volume as well as activation energy represent only strength gradients in the logarithm of viscosity (associated to thermal and pressure gradients, respectively), which necessitates to define a reference viscosity at a given depth and temperature. It has been shown that the effective viscosity at the lithosphere base, corresponding to a minimum if T - and P -dependences are both modelled, is crucial in triggering of small-scale convective processes (e.g. Davaille and Jaupart, 1993; Dumoulin et al., 2001, 2005; Morency et al., 2002), as well as in subduction initiation, as it favors, if low enough, corner flow activation and lubricates the interplate plane base (e.g. Doin and Henry, 2001; Kukačka

Modelling of subduction interplate dynamics

D. Arcay

Title Page

Abstract

Introduction

Conclusions

References

Tables

Figures



Back

Close

Full Screen / Esc

Printer-friendly Version

Interactive Discussion



and Matyska, 2004, 2008). Therefore, I choose to scale ductile strengths with different activation energies and volumes by adjusting the pre-exponential constant, A_0 , in Eq. (2), to keep the asthenosphere viscosity at the lithosphere base, v_{asth} ($z = 100$ km depth, $T = 1350$ °C, $\dot{\epsilon}_{\text{ref}} = 10^{-14}$ s $^{-1}$) equal to 2.724×10^{19} Pas. Nevertheless, the influence of v_{asth} will also be tested by modelling a hydrous strength weakening associated to mantle wedge metasomatism (see Sect. 2.3.1).

Finally, four different ductile rheologies are tested (labelled C6, C10, C12, and C14, Table 2), in order to investigate the respective influence of weak crust activation energy, E_a^c , mantle activation energy, E_a^m , the difference between the latter two, $\Delta E_a = E_a^m - E_a^c$, and the common activation volume of both compositions, V_a . Rheology C6 simulates a weak crust whose strength is close to the undried adirondac granulite studied by Wilks and Carter (1990) and a mantle strength similar to the one of wet synthetic olivine (Karato et al., 1986). Rheologies C6 and C12 are identical except for a small difference in activation volume, and both simulate the ductile behaviours of, respectively, the dry mafic granulite (Wilks and Carter, 1990) for the weak layer, and an intermediate strength between wet dunite at low temperature (Chopra and Paterson, 1981) and wet olivine (Hirth and Kohlstedt, 1996) at high temperature. At last, rheology C13 models a weak crust close to the dry diabase studied by Kirby (1983) and a mantle with a strength similar to wet Aheim dunite at high temperature (Wilks and Carter, 1990) and encompassed at low temperature between wet olivine in Kirby (1983) and wet synthetic olivine in Karato et al. (1986).

Finally, since at least the depth of brittle-ductile transition may depend on interactions between ductile creep and brittle deformation, two strategies are followed to study this possible interplay. On the one hand, the ductile thermo-mechanical parameters are kept constant whereas I vary the crust frictional coefficient (rheologies C10 vs. C10LG; C13 vs. C13HG; C13 vs. C14b, Table 2). On the other hand, the friction parameter is kept constant in rheologies C6 and C12 (and in C13 and C13fnu14) whereas the combinations of ductile rheology parameters are changed.

Modelling of subduction interplate dynamics

D. Arcay

Title Page

Abstract

Introduction

Conclusions

References

Tables

Figures

◀

▶

◀

▶

Back

Close

Full Screen / Esc

Printer-friendly Version

Interactive Discussion



2.4 Numerical resolution

The conservation equations are solved with a spline finite element method on a non-deforming grid (Eulerian approach, Christensen and Yuen, 1984; Christensen, 1992). The simulation box, 2220 km wide and 555 km high, is discretised into 332 × 90 nodes.

- 5 The grid is refined to improve resolution in areas of high thermal and deformation gradients. Close to the subduction plane and in the wedge tip area, the horizontal and depth grid spacings are 2.8 and 2.3 km, respectively. Outside the mantle wedge, they are equal to 9.5 and 10.2 km, respectively. The tracer density is uniform over the simulation box (1 per km²), with a minimum of 7 tracers in the smallest meshes.
- 10 The numerical discretisation used here as well as the tracer density was validated in a former study (Arcay et al., 2005).

3 Interplate dynamics for an old incoming lithosphere

The two following sections describe how the interplate structure evolves as a function of rheological parameters when the subducting lithosphere is old and ~ 100 km thick, i.e., when the strength contrast between the weak interplate material and the surrounding mantle is likely to be maximum. The weak “crust” density is set to 3180 kgm⁻³. The time window is encompassed between 10 and 14 Myr, i.e., close to the end of the subduction transient state, to capture both the main characteristics of the subduction steady-state and the time-evolution of these features.

3.1 Estimate of Z_{BDT} and Z_{dec}

Let us first define the brittle-ductile transition depth, Z_{dec} , and the interplate decoupling depth, Z_{BDT} , in these simulations. Figure 3a illustrates the subduction zone in simulation S13, 16 Myr after simulation start. The subduction interplate domain concentrates deformation (Fig. 3b), and should correspond to a maximum in energy dissipation rate, compared to neighbouring areas. The coordinates of the simulated subduction

SED

4, 943–992, 2012

Modelling of subduction interplate dynamics

D. Arcay

Title Page

Abstract

Introduction

Conclusions

References

Tables

Figures

◀

▶

◀

▶

Back

Close

Full Screen / Esc

Printer-friendly Version

Interactive Discussion



plane are thus extracted by looking for maximum dissipation rates in a window encompassing the converging boundary, and defines the interplate sampling line depicted in Fig. 3a and b. Different mechanical fields are then interpolated along this line: dissipation rates, deviatoric stress, strain rate, and temperature (Fig. 3c). Since brittle strength increases linearly from the surface to a maximum value at the brittle-ductile transition depth, z_{BDT} is easily defined by the depth of maximum stress in stress profiles. I verify that this depth is never higher than the brittle-ductile boundary defined by the relationship $v_v(x, z) = v_b(x, z)$. Above z_{BDT} depth, deformation is mainly ductile and stress decreases while temperature keeps on rising. At the down-dip limit of the subduction plane, the slab surface is in contact with the asthenosphere and there occurs a strong increase in thermal gradient. Asthenospheric rocks becomes then mechanically coupled to the subducting plate. z_{dec} is hence defined by the depth where the strongest temperature increase is recorded along the interplate sampling line, which should also correspond to the location where isotherms at the mantle wedge tip become sub-vertical (Figs. 1a and 3b). As deformation jumps from the subduction interface to the asthenospheric tip at depth $z = z_{\text{dec}}$, we verify that strain rate, dissipation rate and stress are close to zero values in z_{dec} (Fig. 3c).

3.2 Rheological parameters controlling the brittle-ductile transition depth

Figure 4a summarises the simulated z_{BDT} for all rheologies investigated for a 100 Myr old subducting lithosphere, between 10 and 14 Myr after subduction onset. The brittle-ductile transition is usually not yet stabilised in most cases, and either deepens or shallows through time, but the order from the shallowest to the deepest BDT is generally constant, except for the ranks of rheologies C6 and C10 that are a bit more time-dependent. I focus on z_{BDT} obtained 12 Myr after subduction initiation to discuss the effects of rheological parameters.

First, as one may expect, for constant asthenosphere viscosity at the down-dip limit of the subduction plane (i.e., aside rheology C13f14), the BDT depth is mostly dependent on the frictional coefficient, that defines the slope of yield strength increase.

Modelling of subduction interplate dynamics

D. Arcay

Title Page

Abstract

Introduction

Conclusions

References

Tables

Figures

◀

▶

◀

▶

Back

Close

Full Screen / Esc

Printer-friendly Version

Interactive Discussion



z_{BDT} is minimum for the highest friction coefficient ($z_{\text{BDT}} = 49$ km, $\gamma_c = 0.069$, rheology C10) and progressively deepens as γ_c is reduced for rheologies C13HG ($z_{\text{BDT}} = 55$ km, $\gamma_c = 0.061$), C12 ($z_{\text{BDT}} = 58$ km, $\gamma_c = 0.045$), C6 ($z_{\text{BDT}} = 75.3$ km, $\gamma_c = 0.045$), C13 ($z_{\text{BDT}} = 77$ km, $\gamma_c = 0.034$), and C10LG ($\gamma_c = 0.007$, $z_{\text{BDT}} \sim 78$ km but the measurement is quite inaccurate for this extremely low friction coefficient). When friction coefficient decreases, the brittle stress envelops automatically intersects the ductile stress curve at deeper levels (Figs. 1b and 5, compare modelled brittle strengths in simulations S13 and S14b), assuming that the ductile strength is kept more or less constant at a given depth from a simulation to the other. The only exception to this rule is obtained in simulation S14b, where z_{BDT} is always deeper than in simulation S10 (at minimum by 2 km at 12 Myr, up to 16 km at 10 Myr), although friction coefficients are both equal to 0.069. The influence of the weak material activation appears here: if ductile strengths are scaled to maintain an identical asthenosphere viscosity, a lower activation energy ($\Delta E_a^c(\text{C10}) = 335 \text{ kJ mol}^{-1}$, while $\Delta E_a^c(\text{C14b}) = 360 \text{ kJ mol}^{-1}$) is responsible for an interplate viscosity decrease at the same temperature and depth, and yields a z_{BDT} shallowing (as sketched in Fig. 1b). Note that determining z_{BDT} in simulation S14b is difficult, as stress does not directly decrease with depth when the maximum brittle stress is reached, it oscillates around the same maximum value before the creep strength decrease is modelled. The associated uncertainty bars are depicted in Fig. 4a, and suggest that z_{BDT} in simulation S14b still remains deeper than modelled in simulation S10.

The asthenospheric viscosity strongly influences the BDT depth along the subduction interplate. The comparison of simulations S13 and S13f14, that only differs by the mantle viscosity at the mantle wedge tip, clearly shows that z_{BDT} shallows (by ~ 11 km) if asthenosphere viscosity is reduced (here by an imposed water-weakening effect). As depicted in Fig. 4b, the BDT depth equals the interplate decoupling depth at all times in simulations S14b and S13. The interpretation in that specific situation is that the BDT is controlled by the kinematic decoupling depth, z_{dec} (see Sect. 3.4). A softer asthenosphere is more easily entrained by the slab surface, the kinematic coupling between

Modelling of subduction interplate dynamics

D. Arcay

[Title Page](#)[Abstract](#)[Introduction](#)[Conclusions](#)[References](#)[Tables](#)[Figures](#)[◀](#)[▶](#)[◀](#)[▶](#)[Back](#)[Close](#)[Full Screen / Esc](#)[Printer-friendly Version](#)[Interactive Discussion](#)

wedge mantle and subducting plate occurs at shallower levels, which results in a z_{dec} decrease. As a consequence, heating is higher at the subduction plate down-dip extent, and thus softens the weak layer ductile strength, that becomes lower than the brittle strength at shallower depths (Fig. 5, compare simulations S13 and S3f14), and finally brings about the transition from brittle to ductile deformation closer to the trench.

At last, the effect of activation volume on z_{BDT} is suggested by simulations S6 ($V_a = 1.5 \times 10^{-5} \text{ m}^3 \text{ mol}^{-1}$) and S12 ($V_a = 1.7 \times 10^{-5} \text{ m}^3 \text{ mol}^{-1}$), where a z_{BDT} shallowing (by $\sim 6 \text{ km}$, 12 Myr after simulation start) is associated to the activation volume increase. Note that we obtain $z_{\text{BDT}} = z_{\text{dec}}$ in simulation S6 at all times (Fig. 4a and b), and in simulation S12 the BDT and interplate decoupling convergence is modelled at 12 Myr. Therefore, the influence of V_a on z_{BDT} may be the consequence of the interplate decoupling depth dependence in V_a (see Sect. 3.3).

3.3 Rheological parameters controlling the interplate decoupling depth

The modelled interplate decoupling depth is always located in a narrower depth interval than observed for the BDT (between 64 and 92 km depth, whereas the z_{BDT} interval is 40–92 km, Fig. 4b), for all rheologies investigated in this paper. Even if is not completely stable, it is close to steady-state. I focus again on interplate decoupling depths modelled 12 Myr after subduction initiation to discuss the rheological parameter influence.

3.3.1 Parameter with weak influence on z_{dec} : crust friction coefficient

Considering constant asthenospheric viscosities, simulations C13, C13HG, and C14b model very close z_{dec} values (ca. 87 km depth), although their friction coefficients differ. The interplate decoupling depth is thus independent from γ_c (Table 2). Similarly, simulations C10 and C10LG with identical ductile rheological parameters but distinct friction coefficients converge towards the same z_{dec} depth for subduction durations longer than 14 Myr, suggesting that the friction coefficient influence vanishes. Likewise, simulations

Modelling of subduction interplate dynamics

D. Arcay

Title Page

Abstract

Introduction

Conclusions

References

Tables

Figures



Back

Close

Full Screen / Esc

Printer-friendly Version

Interactive Discussion



S10 and S14b with the same crust friction coefficient but different ductile parameters show very different kinematic decoupling depths.

3.3.2 Parameters governing z_{dec} : asthenospheric strength, activation volume, and shift in activation energies between weak crust and mantle

5 As already mentioned in the former section, the viscosity at the lithosphere-asthenosphere boundary has a significant effect on z_{dec} , since the local viscosity decrease applied in simulation S13f14 shallows z_{dec} by ~ 11 km compared with simulation S13. A hydrous viscosity reduction promotes asthenosphere drag by the incoming slab, that in turn, stirs up the return flow along the upper plate base, and heats up the down-dip extent, which eventually weakens the interplate ductile strength at shallower depths (Arcay et al., 2007b, 2008).

As mentioned above, a slight increase in activation volume results in a moderate z_{dec} shallowing (by ~ 6 km) (Fig. 4b). One may remember that the viscosity at the upper plate base is adjusted to be identical in rheology C6 and C12. The lowering in viscosity at the lithosphere-asthenosphere boundary in relation to shallower and deeper strengths should thus be enhanced by a V_a increase, which enhances the corner flow focussing at the mantle wedge tip (Kukačka and Matyska, 2008) and the advected heat flux toward the interplate base, and finally shallows a bit the maximum depth of plate kinematic decoupling.

20 The last parameter affecting the interplate decoupling depth is neither the activation energy of the weak crust material, E_a^c , nor the mantle one, E_a^m , alone, but is the difference between the latter two, ΔE_a , if mantle strength, v_{asth} , at the mantle wedge tip, is unchanged (simulations S6, S12, S13, and S10). Indeed, z_{dec} is minimum for the lowest difference in activation energy between mantle and weak crust ($\Delta E_a = 65 \text{ kJ mol}^{-1}$, $z_{\text{dec}} = 58$ and 64 km, rheologies C12 and C6) and deepens as ΔE_a increases, for rheologies C13, C13HG and C14b ($\Delta E_a = 105 \text{ kJ mol}^{-1}$, $z_{\text{dec}} \sim 87$ km), until its deepest value reached for rheology C10 ($\Delta E_a = 155 \text{ kJ mol}^{-1}$, $z_{\text{dec}} = 92$ km).

Modelling of subduction interplate dynamics

D. Arcay

Title Page

Abstract

Introduction

Conclusions

References

Tables

Figures

◀

▶

◀

▶

Back

Close

Full Screen / Esc

Printer-friendly Version

Interactive Discussion



To understand this result, note that the transition from kinematic decoupling to coupling between the mantle wedge and the subducting plate is controlled by (1) the strength contrast between the interplate domain and the upper lithosphere, and (2) the strength contrast between the subducting slab surface and the mantle wedge. I consider here the interplate segment encompassed between z_{BDT} and z_{dec} in the ductile realm.

The strength contrast between crust material and the surrounding mantle is basically governed by strain rate (non-Newtonian rheology), geotherm, and ΔE_a . Although the weak crust material is, by definition, weaker than the mantle in the ductile domain at the same pressure, temperature and strain rate conditions, note that the interplate geotherm is much colder than a classical vertical geotherm across a 100 km thick oceanic lithosphere (see Fig. 3c4), which makes the weak crustal material at depths shallower than z_{dec} stronger than the upper lithosphere mantle located at the same depth, but far enough from the subduction zone to remain undisturbed. The weak crustal material nevertheless localises deformation along the subduction interface because it remains much weaker than both the underlying very cold subducting lithospheric mantle, and the fore-arc mantle, cooled and underformed, and therefore very viscous (see Fig. 1b). At the depth $z = z_{\text{dec}}$, the deficit in temperature between cold interplate channel and hot asthenosphere is abruptly recovered, and, as a consequence, reverses the strength order between weak crust and the classical upper lithospheric mantle. The z_{dec} simulated here corresponds to the depth where the crust layer stress profile crosses the mantle one.

The contrast between mantle and crust strengths is directly dependent on ΔE_a : strongest mantle and weakest crust for rheology C10 ($\Delta E_a = 155 \text{ kJ mol}^{-1}$), weakest mantle and strongest crust for rheology C12 ($\Delta E_a = 65 \text{ kJ mol}^{-1}$). To sum up, crust and overlying mantle strengths are the closest for the lowest ΔE_a value, and their crossing is therefore favored at lower temperature contrary to a high ΔE_a situation. Besides, the strength contrast between the weak crustal material and the underlying subducting cold mantle, is similarly controlled by ΔE_a . Hence, a high ΔE_a favors kinematic decoupling

between the subducting lithospheric mantle and the overlying upper plate, and thus promotes deeper Z_{dec} .

Note that, however, the corner flow is active if asthenosphere can be successfully dragged downward by the slab which can occur if the dragging layer at the slab-asthenosphere contact is more viscous than the mantle wedge medium (as clearly evidenced by Kukačka and Matyska, 2008). It is in fact the subducting slab-induced cooling that is responsible for this dragging (“viscous blanket” formation, Kincaid and Sacks, 1997, see also Fig. 1), or, in other words, the “lithospherisation” of the asthenosphere at the crust surface that trigger the downward drag.

One may wonder if the interplate geotherm finally governs the location of maximum kinematic decoupling. From the surface to $z = Z_{\text{dec}}$, temperature within the interplate channel is strongly affected by the friction coefficient, as γ_c controls the shearing stress, and thus the rate of dissipated energy (Fig. 6a), if the strain rate remains roughly controlled by the constant convergence rate. As a consequence, dissipation rate increases from simulation S13 ($23.7 \mu\text{W m}^{-3}$, 50 km depth, $\gamma_c = 0.034$) to simulations S6 and S12 ($28.4 \mu\text{W m}^{-3}$, $\gamma_c = 0.045$), to a maximum in simulation S10 ($39 \mu\text{W m}^{-3}$, $\gamma_c = 0.069$). This results in a significant temperature difference (up to $\sim 100^\circ\text{C}$) along the subduction interplate, as illustrated in Fig. 6b, 12 Myr after simulation start ($T = 454^\circ\text{C}$ in simulation S10 at a depth of 50 km and only 346°C in simulation S13). Hence the brittle behaviour indirectly affects the interplate decoupling depth by modifying the interplate geotherm. The dissipation energy associated to brittle deformation would rather act as an accelerating factor than a decoupling trigger, actually. Indeed, in simulation S10LG performed with an extremely low friction coefficient, the dissipation rate along the subduction interface and thence temperature are very low with respect to other simulations (Fig. 6). The interplate decoupling depth requires a longer subduction duration to reach a stable location, but finally stabilizes at the same depth as the one modelled in simulation S10 (Fig. 4b). I conclude that it is the thermomechanical equilibrium at the down-dip extent of the interplate plane/mantle wedge tip that finally governs the interplate decoupling depth, and not the brittle behaviour occurring at shallow depths.

Modelling of subduction interplate dynamics

D. Arcay

[Title Page](#)[Abstract](#)[Introduction](#)[Conclusions](#)[References](#)[Tables](#)[Figures](#)[⏪](#)[⏩](#)[◀](#)[▶](#)[Back](#)[Close](#)[Full Screen / Esc](#)[Printer-friendly Version](#)[Interactive Discussion](#)

3.4 Conditions favoring $Z_{\text{dec}} = Z_{\text{dec}}$

The BDT and the end of kinematic decoupling between the two converging plates occur at the same depth, already 10 Myr after subduction initiation, in simulations S13 and S13f14, and from 12 Myr in simulations S6, S12 and S10LG (Fig. 4). In all cases the friction coefficient is low (at maximum equal to 0.045 in simulations S6 and S12, Table 2). A (relatively) high friction coefficient automatically yields high shear stresses, that exceed ductile stress at shallow depths and impedes brittle deformation. A very low friction is hence necessary to sustain brittle behaviour at deep levels. The transition from brittle to creep deformation is then forced by the sudden high temperature increase in the vicinity of the asthenosphere. The BDT depth would thus be controlled by the decoupling depth location, rather than the contrary. Simulation S6 shows that the weak material filling the interplate boundary has a mechanical behaviour mainly brittle all along the converging boundary. Its upper part jumps in the ductile domain exactly at the depth $z = z_{\text{dec}}$ (Fig. 7). The governing influence of corner flow in cases where $Z_{\text{BDT}} = z_{\text{dec}}$ is also suggested by the comparison of interplate stress between simulations S13 and S13f14 (Fig. 5), where a low asthenospheric strength promotes a shallower z_{dec} and shallows consequently the BDT. To conclude, the situation where the BDT occurs at the downdip extent of the interplate plane is conditioned by, first, a low interplate friction coefficient, and second, favors by low asthenosphere viscosities at the mantle wedge tip. It is however far from being a general case, as initially assumed by Arcay et al. (2007a,b).

4 Interplate dynamics for a young incoming lithosphere

In this section, the initiation of a young and hot lithosphere subduction under a 100 km thick upper plate is investigated as a function of the rheological parameter set. The model set up is depicted in Fig. 2b. The same rheologies as in the previous section are tested. The influence of the weak layer density is also tested in a few simulations.

Before presenting the modelling results, a synthesis from models of old plate subduction is briefly summed up to discuss what main factors are likely to be the most sensitive in young subducting lithosphere modelling.

4.1 Parameters favoring the interplate kinematic decoupling for an old subducting lithosphere: critical factors for the initiation of a hot lithosphere subduction

The kinematic decoupling between the two converging plates is efficient all along the interplate plane if the weak material filling the modelled channel is significantly weaker than both the underlying subducting lithospheric mantle and the overlying fore-arc mantle. This is carried out from the surface to the BDT depth thanks to the low brittle yield strength. In the ductile part of the interplate plane (for $z_{BDT} < z \leq z_{dec}$), the deformation localisation is promoted by a high difference in activation energy between the interplate layer and the surrounding mantle. Localisation is besides helped by the non-Newtonian strength, decreasing in high strain rate areas, that focuses deformation within highly deforming and low strength layers. Since temperature continuously increases with depth, the viscous strength and stress progressively decreases, until a sharp temperature increase at the asthenosphere contact that reduces drastically stresses. High strain rates along the interplate plane there separates in two main branches (Fig. 1b), one at the viscous blanket surface where the asthenosphere is sheared by slab drag, and the second spreading out along the upper plate base where the upper part of the corner flow takes place. The corner flow efficiency is here crucial because the advected heat flux is responsible for lubricating the interplate base and enhancing the kinematic decoupling at the upper plate sublayer where mantle is hot and soft. The kinematic decoupling stops at $z = z_{dec}$ because strength and stress are so low that the weak layer material is not weak enough anymore to decouple the slab motion from the low viscosity asthenosphere. Note that the kinematic decoupling at the down-dip interplate extent is promoted if $z_{BDT} = z_{dec}$ because shear heating associated to brittle deformation contributes to decrease stress.

For a young subducting lithosphere, one may expect that the kinematic decoupling in the deep ductile interplate part is complicated by the hotter subducting thermal state, that reduces on one hand the downward slab pull that verticalises the convergent motion, and, on the other hand, lessens the thermal gradient between subducting slab and hot asthenosphere, and thus the viscous drag efficiency. To test the first point, different density of the weak crust layer are tested. The second one might be partly compensated if a low viscosity is added at the mantle wedge tip.

4.2 Results: convergence mode of a young subducting lithosphere – influence of rheology

The subduction of a 20 Myr old (~ 50 km thick) lithosphere under a 100 km thick lithosphere is performed with the five rheological sets discussed in Sect. 3 (C6, C10, C12, C13, and C14b) with different weak layer densities. Two additional tests are performed with a decreased asthenospheric viscosity.

The subduction process initiates nicely in simulations S10b, S13b, and S14b. The kinematic decoupling between the two converging plates, and the kinematic coupling with the corner flow stir up and make the subduction process sustainable (Fig. 8a). On the contrary, in simulations S6, S12, and S12b2, the subduction process at the interplate down-dip extent slows down and eventually get jammed along the sublithospheric layer. In these three cases, the interplate plane is locked very soon (in less than 6 Myr after simulation start) while convergence at the down-dip extent, initially with a 30° dipping angle, progressively becomes horizontal (Fig. 8b). As a consequence, the downward asthenosphere drag at the subducting slab surface stops, and the upper branch of the corner flow necessary to heat and decouple mechanically the slab surface from the upper plate base is not active any more. The previously subducted slab is thermally weakened and finally drips.

Simulations S6 and S12b are performed with a weak crust density lower than the mantle density (-190 and -80 kg m^{-3} , respectively, Table 2), but the crust buoyancy is set to zero in simulation S12b2 without improving the subduction interplate functioning.

The weak layer thickness generally thins a bit at the interplate decoupling depth, mainly because the subducting slab is locally stretched by its bending (as also modelled in a cold subducting lithosphere, Fig. 8a). In simulation S12, the weak crust is not able to dig efficiently its own way toward the asthenosphere and accumulates at shallower levels, which automatically jams the interplate base. However, this is not observed in simulations S6 and S12b. The weak layer thinning is also observed in successfully initiated subduction (see for instance Fig. 8a). Interplate geotherms in simulations S6, S12, and S12b2 are always close to those simulated in simulations S10b, S13b, and S14b. This suggests that it may not be the interplate geotherm that governs alone the efficiency of the interplate kinematic decoupling but the strength contrast between mantle and crust associated to it. The three simulations showing a jammed basal interplate are also the three ones with the lowest ΔE_a . Decreasing the asthenospheric viscosity while the difference between mantle and crust activation energy is low is not sufficient to trigger the kinematic decoupling. The difference in activation energy set between the weak localising material and the surrounding mantle thus appear to be a basic parameter to model a successful initiation of subduction in this set-up. However, if a high ΔE_a might promote the interplate kinematic decoupling in the vicinity of hot basal upper lithosphere, note that a too high ΔE_a could result in a buoyant crustal layer too soft to remain attached to the slab, if eclogitization is not modelled.

4.3 Interplate geometry for a young incoming lithosphere – comparison to an old plate subduction

Figure 9 compares the BDT and the interplate decoupling depths modelled 12 Myr after subduction initiation, for both a 18 Myr old and 100 Myr old subducting lithospheres. Rheologies which fail to simulate subduction of a hot subducting lithosphere are not included. The particular situation $z_{\text{dec}} = z_{\text{BDT}}$ is never modelled for a young incoming plate. The subducting lithosphere ageing deepens a bit the BDT depth for high friction coefficients (by only 5 km, rheologies C10 and C14b) which can directly be related to the interplate geotherm cooling. The z_{BDT} deepening is significant in the only case of

Modelling of subduction interplate dynamics

D. Arcay

Title Page

Abstract

Introduction

Conclusions

References

Tables

Figures

◀

▶

◀

▶

Back

Close

Full Screen / Esc

Printer-friendly Version

Interactive Discussion



a very low friction coefficient (rheology C13, z_{BDT} deepening of 25 km) because a low friction coefficient maintains very low stresses to high depths, that are reached in the ductile realm only for very hot (and thus deep) temperatures.

Regarding the decoupling depth, surprisingly, it shallows for cold and old subducting lithospheres (by ~ 10 km and 17 km, respectively, for rheologies C13 and C14b, respectively). This effect is likely to be related to the higher rigidity of the viscous blanket for an old subducting plate, associated to a high temperature gradient at the slab surface, able to mobilise a thicker layer of hot asthenosphere, and thus emphasizing the corner flow effect on the interplate base weakening at shallower levels. This effect is tiny in the case of rheology C10, where z_{dec} is very deep and already close to the upper plate thickness for an old subducting lithosphere, and cannot be so much deepened during the young lithosphere subduction (deepening of ~ 3 km between $A_{\text{lith}} = 100$ Myr and $A_{\text{lith}} = 18$ Myr).

4.4 Consequences on subduction initiation and perennity

To test the viability of the subduction system, the compressive force exerted by the kinematic boundary condition to sustain a constant convergence rate of 6.5 cm yr^{-1} is computed as deviation of horizontal deviatoric stresses, σ_{xx} , from hydrostatic stresses in an oceanic column of density ρ_{ref} (Christensen, 1992):

$$F_s = - \int_0^{z_c} \sigma_{xx} dz + \int_0^{z_c} \rho_{\text{ref}}(z) z g dz \quad (3)$$

where z_c is the compensation depth (259 km depth). $F_s > 0$ indicates a compressive stress state. Subduction is realistically modelled if F_s remains by the order of natural tectonic forces, that is, not higher than 10^{13} Nm^{-1} . This force becomes rapidly excessively high when the subduction interplate stops decoupling the two converging plate motions, as simulated in simulations S6b and S12b (Fig. 10). Setting to zero

Modelling of subduction interplate dynamics

D. Arcay

Title Page

Abstract

Introduction

Conclusions

References

Tables

Figures



Back

Close

Full Screen / Esc

Printer-friendly Version

Interactive Discussion



the weak layer buoyancy has no effect on the extremely high exerted compression (simulation S12b2). However, a zero density contrast between weak crust and mantle, $\Delta\rho_c$, is required to maintain the applied force to subduct to an acceptable level with rheology C13, even if (1) the subduction interplate decoupling properly works and (2) the weak crust friction coefficient is low. The alternative to sustain a realistic compressive force (but still high, by $\sim 6.7 \times 10^{12} \text{ Nm}^{-1}$) on the subduction zone is to decrease the asthenosphere strength in the mantle wedge tip (rheology C13f14). At last, note that the weak layer friction coefficient strongly increases the force resistant to subduction: close to steady-state subduction, $F_s \sim 2.8 \times 10^{12} \text{ Nm}^{-1}$ in simulation S13 ($\gamma_c = 0.034$, $\Delta\rho_c = 0 \text{ kg m}^{-3}$) increases to $F_s \sim 7.3 \times 10^{12} \text{ Nm}^{-1}$ in simulation S14b, ($\gamma_c = 0.069$, $\Delta\rho_c = 0 \text{ kg m}^{-3}$).

5 Discussion

5.1 Friction coefficient within the interplate shear zone

The coefficient of friction characterising a subduction fault plane is still a matter of debate and one may wonder if the low to very low friction coefficients investigated here are realistic. Numerous studies of lithosphere convergence argue for friction coefficients along the plate boundary higher than 0.2, such as in Northern Chile (Delouis et al., 1998), Himalaya (Cattin and Avouac, 2000), Andaman-Sumatra subduction zone (Cattin et al., 2009), as also suggested by accretionary/non-accretionary wedge dynamics (Lallemand et al., 1994). On the contrary, very low frictional coefficients ($0.05 \leq \gamma_c < 0.09$ and even $\gamma_c = 0.03$) have been invoked to explain low stress state in Cascadia, Kermadec, NE and SW Japan subduction zones (Wang et al., 1995; Wang and Suyehiro, 1999; Wang and He, 1999; von Herzen et al., 2001) or low shear stresses estimates from subduction megathrusts (Lamb, 2006). Similarly, Tichelaar and Ruff (1993) assume low friction coefficients ($0.047 \leq \gamma_c < 0.13$) to predict shear stresses along the subduction plane from heat flow data inversion. Such

Modelling of subduction interplate dynamics

D. Arcay

Title Page

Abstract

Introduction

Conclusions

References

Tables

Figures

◀

▶

◀

▶

Back

Close

Full Screen / Esc

Printer-friendly Version

Interactive Discussion



Modelling of subduction interplate dynamics

D. Arcay

Title Page

Abstract

Introduction

Conclusions

References

Tables

Figures

◀

▶

◀

▶

Back

Close

Full Screen / Esc

Printer-friendly Version

Interactive Discussion



low coefficients of effective friction could result from high pore pressures and porosity down to a few tens of kilometers depth, as suggested in the NE Japan subduction zone (Magee and Zoback, 1993) and in the Cascadia subduction zone (Peacock et al., 2011). Besides, numerical models of dynamic subduction simulating realistic viscoplastic rheology (even including sometimes elasticity) revealed that a low strength interplate plane ($\gamma_c < 0.1$) is required to model convergence of strong lithospheres (Hassani et al., 1997; Hall and Gurnis, 2003; Sobolev and Babeyko, 2005; Tagawa et al., 2007; Gorczyk et al., 2007). Gerya et al. (2008) show that a very high strength contrast between converging plates and the sheared interplate material, favored by a interplate friction coefficient close to zero, is necessary to model one-sided subduction over a wide range of subducting lithosphere age.

This suggests obviously a probable strong variation of friction properties from a subduction plane to another, depending on the local lithology, stratigraphy and thermal state. One possible way to reconcile high and low friction coefficient estimate might be to test a friction coefficient significantly varying with depth, as a function of the temperature, fluid pressure, and metamorphic reactions.

5.2 BDT and subduction decoupling depth in nature

A lower boundary for z_{BDT} can be inferred from the maximum seismogenic depth along the subduction interface. The maximum depth of seismic coupling was initially though to be restricted to 40 km depth (Ruff and Kanamori, 1983), but more recent studies suggest a broader interval, between 20–55 km (Tichelaar and Ruff, 1993) and up to 35 to 70 km (Pacheco et al., 1993, based a 19 subduction zones), which was recently confirmed by a worldwide subduction catalogue analysis (Heuret et al., 2011), well beyond the upper plate Moho depth in 70 % of subduction zones. Recent subduction megathrust earthquakes also suggest a seismogenic slip up to 55 km depth (Lay et al., 2012).

Taking this seismogenic coupling depth range as an upper bound for the BDT depth in the present modelling, this imposes a friction coefficient for the interplate plane medium at least equal to $\gamma_c = 0.045$ to simulate $z_{BDT} \leq 65$ km if hydrated

asthenosphere viscosity decrease is excluded (rheology C6, Fig. 4b). The occurrence of $z_{\text{BDT}} = z_{\text{dec}}$ (BDT governed by the depth of kinematic coupling between subducting plate and asthenosphere flows) is then highly unlikely, except if the mantle wedge presents a low viscosity, possibly sustained by the diving slab dehydration and mantle wedge metasomatism, which besides questions the amount of necessary strength reduction associated to fluid permeation.

How to constrain the interplate decoupling depth in this model? An accurate comparison between the interplate decoupling depth modelled in a self-consistent thermo-mechanical equilibrium, with a freely evolving dip angle, and observations in very specific subduction condition (age of the subducting plates, speed and angle of convergence, structure of the fore-arc lithosphere,...) is beyond the scope of this study. Recalling that z_{dec} is highly dependent on convergence rate (deepening for fast subduction, shallowing for slow convergence Arcay et al., 2007b, 2008), but also on the mantle wedge viscosity, and incoming lithosphere age, as showed in this paper, the objective in this section is simply to evaluate the validity of the z_{dec} depth range modelled here by looking at a few well-documented subduction zones.

Two main types of geophysical data may be looked at, seismic wave (attenuation) tomography and heat flows profiles. Abers et al. (2006) show that the sharp lateral transition between hot asthenosphere at the mantle tip and the cooled fore-arc nose on-top of the cold subducting slab surface is likely to be revealed by an abrupt increase in seismic wave velocities and/or in seismic wave attenuation, as observed in the subduction zones of NE Japan, Cascadia, and Alaska (Zhao et al., 1992, 2001; Stachnik et al., 2004). z_{dec} would then be inferred at a depth of ~ 45 km at minimum in the Cascadia, ~ 65 km in the Alaska subduction zone, and possibly around 65 km in the NE Japan subduction zone. It is however difficult to interpret definitely the transition from high to low seismic wave velocity in the vicinity of the slab surface in term of temperature increase close to the asthenospheric mantle wedge, as low seismic velocity anomalies may be related to partial melting, possibly compatible with high temperatures, or on the contrary to serpentinisation in the cooled fore-arc lithospheric mantle

Modelling of subduction interplate dynamics

D. Arcay

[Title Page](#)[Abstract](#)[Introduction](#)[Conclusions](#)[References](#)[Tables](#)[Figures](#)[⏪](#)[⏩](#)[◀](#)[▶](#)[Back](#)[Close](#)[Full Screen / Esc](#)[Printer-friendly Version](#)[Interactive Discussion](#)

trench, would rather suggest a shallower z_{dec} , encompassed between 40 and 50 km depth. At last, the heat flow maximum in the fore-arc area is detected ~ 270 km away from the trench in the Mexico subduction zone (70 mW m^{-2} , Ziagos et al., 1985), and would correspond to a slab-upper plate decoupling at 120 km depth following the subduction geometry proposed by Currie et al. (2002). Yet, Wada and Wang (2009) model a much shallower value, close to 60 km, in their thermo-kinematic simulation.

The final depth range for z_{dec} would then be from 50 km to a bit more than ~ 100 km depth, with a recurrent observed value around 70 km, which is a bit less and a bit more than the depth interval simulated in this paper (Fig. 4b). Convergence rates higher than 6.5 cm yr^{-1} would lead to decoupling depths shallower than simulated here, whereas low convergence rates (1 cm yr^{-1}) deepen z_{dec} to more than 120 km. I therefore conclude that the z_{dec} modelling proposed here simulates realistic down-dip extents of the subduction interplate plane, and has the basic advantage to model a self-consistent interplate dynamics.

6 Conclusions

By combining a non-Newtonian viscous rheology and a pseudo-brittle rheology, thermomechanical models are performed to model the long-term equilibrium state of a subduction interplate. The subduction interplate dynamics is shown to be strongly dependent on both ductile and brittle strength parameters. For an old subducting lithosphere, the brittle-ductile transition depth mainly depends on the friction coefficient and the activation energy of the interplate material. If the BDT occurs at the kinematic decoupling depth, it is then affected by the depth-dependence of the ductile strength and the asthenosphere strength at the mantle wedge tip. The kinematic decoupling depth along the subduction plane is highly sensitive to the viscosity in the mantle wedge, the activation volume of the ductile strength, and the difference in activation energy between mantle and interplate material. Deep BDT can be simulated at the depth of interplate kinematics only if very low interplate friction coefficients are modelled, and/or

Modelling of subduction interplate dynamics

D. Arcay

Title Page

Abstract

Introduction

Conclusions

References

Tables

Figures

◀

▶

◀

▶

Back

Close

Full Screen / Esc

Printer-friendly Version

Interactive Discussion



if a decrease in asthenosphere strength, possibly associated to metasomatism, is included. A high contrast between mantle activation energy and the one of interplate medium is besides necessary to simulate a realistic subduction of a 20 Myr old plate. Finally, both the BDT depth and the decoupling depth depend on the subducting plate age, but are not influenced in the same fashion: cool and old subducting plates deepen the BDT but shallow the interplate decoupling depth. Even if BDT and kinematic decoupling are intrinsically related to different mechanisms of deformation, this work shows that they are able to closely interact.

Acknowledgements. I thank Serge Lallemand et Arnaud Heuret for stimulating discussions on subduction dynamics and its mysterious interplate, and Susanne Buitert for having solicited me to attend EGU 2011 in Vienna, which ended with this paper. I express here my gratitude to Matthieu and Izia Lilla for their warming support. This research was supported by the CNRS-INSU SYSTER program 2010–2011.



The publication of this article is financed by CNRS-INSU.

References

- Abers, G., van Keken, P., Kneller, E., Ferris, A., and Stachnik, J.: The thermal structure of subduction zones constrained by seismic imaging: slab dehydration and wedge flow, *Earth Planet. Sci. Lett.*, 241, 387–397, 2006. 970, 971
- Andrews, D. and Sleep, N.: Numerical modelling of tectonic flow behind island arcs., *Geophys. J. R. Astron. Soc.*, 38, 237–251, 1974. 947

SED

4, 943–992, 2012

Modelling of subduction interplate dynamics

D. Arcay

Title Page

Abstract

Introduction

Conclusions

References

Tables

Figures

⏪

⏩

◀

▶

Back

Close

Full Screen / Esc

Printer-friendly Version

Interactive Discussion



Modelling of subduction interplate dynamics

D. Arcay

Title Page

Abstract

Introduction

Conclusions

References

Tables

Figures

◀

▶

◀

▶

Back

Close

Full Screen / Esc

Printer-friendly Version

Interactive Discussion



- Arcay, D., Tric, E., and Doin, M.-P.: Numerical simulations of subduction zones: effect of slab dehydration on the mantle wedge dynamics, *Phys. Earth Planet. Inter.*, 149, 133–153, 2005. 953, 956
- Arcay, D., Doin, M.-P., and Tric, E.: Overriding plate thinning in subduction zones: localized convection induced by slab dehydration, *Geochem. Geophys. Geosyst.*, 7, Q02007, doi:10.1029/2005GC001061, 2006. 953
- Arcay, D., Doin, M.-P., Tric, E., and Bousquet, R.: Influence of the precollisional stage on the subduction dynamics and the buried crust thermal state: insights from numerical simulations, *Tectonophysics*, 441, 27–45, doi:10.1016/j.tecto.2007.06.001, 2007a. 948, 963
- Arcay, D., Tric, E., and Doin, M.-P.: Slab surface temperature in subduction zones: influence of the interplate decoupling depth and upper plate thinning processes, *Earth Planet. Sci. Lett.*, 255, 324–338, doi:10.1016/j.epsl.2006.12.027, 2007b. 948, 960, 963, 970
- Arcay, D., Lallemand, S., and Doin, M.-P.: Back-arc strain in subduction zones: statistical observations vs. numerical modelling, *Geochem. Geophys. Geosyst.*, 9, Q05015, doi:10.1029/2007GC001875, 2008. 948, 960, 970
- Audet, P., Bostock, M., Christensen, N., and Peacock, S.: Seismic evidence for over-pressured subducted oceanic crust and megathrust fault sealing, *Nature*, 457, 76–78, doi:10.1038/nature07650, 2009. 948
- Billen, M. and Gurnis, M.: A low viscosity wedge in subduction zones, *Earth Planet. Sci. Lett.*, 193, 227–236, 2001. 946
- Billen, M. and Gurnis, M.: Constraints on subducting plate strength within the Kermadec trench, *J. Geophys. Res.*, 110, B05407, doi:10.1029/2004JB003308, 2005. 953
- Bostock, M. and van Decar, J.: Upper mantle structure of the Northern Cascadia subduction zone, *Can. J. Earth Sci.*, 32, 1–12, 1995. 971
- Bostock, M., Hyndman, R., Rondenay, S., and Peacock, S.: An inverted continental Moho and serpentinization of the forearc mantle, *Nature*, 417, 536–538, 2002. 971
- Branlund, J., Regenauer-Lieb, K., and Yuen, D.: Weak zone formation for initiating subduction from thermo-mechanical feedback of low-temperature plasticity, *Earth Planet. Sci. Lett.*, 190, 237–250, 2001. 948
- Brocher, T., Parsons, T., Tréhu, A., Snelson, C., and Fisher, M.: Seismic evidence for widespread serpentinized forearc upper mantle along the Cascadia margin, *Geology*, 31, 267–270, 2003. 971

Modelling of subduction interplate dynamics

D. Arcay

[Title Page](#)
[Abstract](#)
[Introduction](#)
[Conclusions](#)
[References](#)
[Tables](#)
[Figures](#)
[Back](#)
[Close](#)
[Full Screen / Esc](#)
[Printer-friendly Version](#)
[Interactive Discussion](#)


- Cattin, R. and Avouac, J.: Modeling mountain building and the seismic cycle in the Himalaya of Nepal, *J. Geophys. Res.*, 105, 13389–13407, 2000. 968
- Cattin, R., Chamot-Rooke, N., Pubellier, M., Rabaute, A., Delescluse, M., Vigny, C., Fleitout, L., and Dubernet, P.: Stress change and effective friction coefficient along the Sumatra-Andaman-Sagaing fault system after the 26 December 2004 ($M_w = 9.2$) and the 28 March 2005 ($M_w = 8.7$) earthquakes, *Geochem. Geophys. Geosyst.*, 10, Q03011, doi:10.1029/2008GC002167, 2009. 968
- Chopra, P. and Paterson, M.: The experimental deformation of dunite, *Tectonophysics*, 78, 453–473, 1981. 955
- Christensen, U. and Yuen, D.: The interaction of a subducting lithosphere slab with a chemical of phase boundary, *J. Geophys. Res.*, 89, 4389–4402, 1984. 949, 956
- Christensen, U. R.: Convection with pressure- and temperature-dependent non-Newtonian rheology, *Geophys. J. R. Astron. Soc.*, 77, 343–384, 1984. 954
- Christensen, U. R.: An Eulerian technique for thermomechanical modeling, *J. Geophys. Res.*, 97, 2015–2036, 1992. 949, 956, 967
- Collot, J.-Y., Ribodetti, A., and Sage, F.: The South Ecuador subduction channel: evidence for a dynamic mega-shear zone from 2D fine-scale seismic reflection imaging and implications for material transfer, *J. Geophys. Res.*, 116, B11102, doi:10.1029/2011JB008429, 2011. 948
- Conder, J.: A case for hot slab surface temperatures in numerical viscous flow models of subduction zones with an improved fault zone parameterization, *Phys. Earth Planet. Inter.*, 149, 155–164, 2005. 946, 948
- Currie, C., Hyndman, R., Wang, K., and Kostoglodov, V.: The thermal of the Mexico subduction zone: implications for the megathrust seismogenic zone, *J. Geophys. Res.*, 107, 2370, doi:10.1029/2001JB000886, 2002. 972
- Currie, C., Wang, K., Hyndman, R., and He, J.: The thermal effects of steady-state slab-driven mantle flow above a subducting plate: the Cascadia subduction zone and backarc, *Earth Planet. Sci. Lett.*, 223, 35–48, 2004. 971
- Davaille, A. and Jaupart, C.: Transient high-Rayleigh number thermal convection with large viscosity variations, *J. Fluid. Mech.*, 253, 141–166, 1993. 954
- Davies, E. and Lewis, T.: Heat flow in a back-arc environment: Intermontane and Omineca crystalline belts, *Southern Canadian Cordillera*, *Can. J. Earth Sci.*, 21, 715–726, 1984. 971

Modelling of subduction interplate dynamics

D. Arcay

Title Page

Abstract

Introduction

Conclusions

References

Tables

Figures

◀

▶

◀

▶

Back

Close

Full Screen / Esc

Printer-friendly Version

Interactive Discussion



- Delouis, B., Philip, H., Dorbath, L., and Cisternas, A.: Recent crustal deformation in the Antofagasta region (Northern Chile) and the subduction process, *Geophys. J. Int.*, 132, 302–338, 1998. 968
- Doin, M.-P. and Fleitout, L.: Thermal evolution of the oceanic lithosphere: an alternative view, *Earth Planet. Sci. Lett.*, 142, 121–136, 1996. 952
- Doin, M.-P. and Henry, P.: Subduction initiation and continental crust recycling: the roles of rheology and eclogitization, *Tectonophysics*, 342, 163–191, 2001. 949, 954
- Dumoulin, C., Doin, M.-P., and Fleitout, L.: Heat transport in stagnant lid convection with temperature- and pressure-dependent Newtonian or non-Newtonian rheology, *J. Geophys. Res.*, 104, 12759–12778, 1999. 954
- Dumoulin, C., Doin, M.-P., and Fleitout, L.: Numerical simulations of the cooling of an oceanic lithosphere above a convective mantle, *Phys. Earth Planet. Inter.*, 125, 45–64, 2001. 954
- Dumoulin, C., Doin, M.-P., Arcay, D., and Fleitout, L.: Onset of small-scale instabilities at the base of the lithosphere: scaling laws and role of pre-existing lithospheric structures, *Geophys. J. Int.*, 160, 344–356, 2005. 954
- Eberle, M., Grasset, O., and Sotin, C.: A numerical study of the interaction between the mantle wedge, the subducting slab, and overriding plate, *Phys. Earth Planet. Inter.*, 134, 191–202, 2002. 946
- Faccenda, M., Gerya, T., and Chakraborty, S.: Styles of post-subduction collisional orogeny: influence of convergence velocity, crustal rheology and radiogenic heat production, *Lithos*, 103, 257–287, doi:10.1016/j.lithos.2007.09.009, 2008. 949
- Flück, P., Hyndman, R., and Wang, K.: 3-D dislocation model for great earthquakes of the Cascadia subduction zone, *J. Geophys. Res.*, 102, 20539–20550, 1997. 971
- Furukawa, Y.: Depth of the decoupling plate interface and thermal structure under arcs, *J. Geophys. Res.*, 98, 20005–20013, 1993. 946, 947, 971
- Gerya, T., Connolly, J., and Yuen, D.: Why is terrestrial subduction one-sided?, *Geology*, 36, 43–46, 2008. 969
- Gorczyk, W., Willner, A., Gerya, T., Connolly, J., and Burg, J.-P.: Physical controls of magmatic productivity at Pacific-type convergent margins: new insights from numerical modeling, *Phys. Earth Planet. Inter.*, 163, 209–232, doi:10.1016/j.pepi.2007.05.010, 2007. 969
- Hall, C. and Gurnis, M.: Catastrophic initiation of subduction following forced convergence across fracture zones, *Earth Planet. Sci. Lett.*, 212, 15–30, 2003. 969

Modelling of subduction interplate dynamics

D. Arcay

Title Page

Abstract

Introduction

Conclusions

References

Tables

Figures

◀

▶

◀

▶

Back

Close

Full Screen / Esc

Printer-friendly Version

Interactive Discussion



- Kukačka, M. and Matyska, C.: Influence of the zone of weakness on dip angle and shear heating of subducted slabs, *Phys. Earth Planet. Inter.*, 141, 243–252, 2004. 954
- Kukačka, M. and Matyska, C.: Numerical models of heat flow in back-arc regions, *Earth Planet. Sci. Lett.*, 276, 243–252, 2008. 955, 960, 962
- 5 Lallemand, S.: High rates of arc consumption by subduction processes: some consequences, *Geology*, 23, 551–554, 1995. 948
- Lallemand, S., Schnürle, P., and Manoussis, S.: Reconstruction of subduction zone paleogeometries and quantification of upper plate material losses caused by tectonic erosion, *J. Geophys. Res.*, 97, 217–239, 1992. 948
- 10 Lallemand, S., Schnürle, P., and Malavieille, J.: Coulomb theory applied to accretionary and nonaccretionary wedges: possible causes for tectonic erosion and/or frontal accretion, *J. Geophys. Res.*, 99, 12033–12056, doi:10.1029/94JB00124, 1994. 968
- Lamb, S.: Shear stresses on megathrusts: implications for mountain building behind subduction zones, *J. Geophys. Res.*, 111, B07401, doi:10.1029/2005JB003916, 2006. 968
- 15 Langseth, M., Hobart, M., and Horai, K.: Heat flow in the Bering Sea, *J. Geophys. Res.*, 85, 3740–3750, 1980. 971
- Lay, T., Kanamori, H., Ammon, J., Koper, K., Hutko, A., Ye, L., Yue, H., and Rushing, T.: Depth-varying rupture properties of subduction zone megathrust faults, *J. Geophys. Res.*, 117, doi:10.1029/2011JB009133, 2012. 969
- 20 Lewis, T., Bentkowski, W., Davis, E., Hyndman, R., Souther, J., and Wright, J.: Subduction of the Juan de Fuca Plate: thermal consequence, *J. Geophys. Res.*, 93, 15207–15227, 1988. 971
- Lewis, T., Bentkowski, W., and Hyndman, R.: Crustal temperatures near the Lithoprobe corridor Southern Canadian Cordillera Transect, *Can. J. Earth Sci.*, 29, 1197–1214, 1992. 971
- 25 Magee, M. and Zoback, M.: Evidence for a weak interplate thrust fault along the Northern Japan subduction zone and implications for the mechanics of thrust faulting and fluid expulsion, *Geology*, 21, 809–812, 1993. 969
- Morency, C., Doin, M.-P., and Dumoulin, C.: Convective destabilization of a thickened continental lithosphere, *Earth Planet. Sci. Lett.*, 202, 303–320, 2002. 954
- 30 Obara, K.: Nonvolcanic deep tremor associated with subduction in Southwest Japan, *Science*, 296, 1679–1681, 2002. 948
- Pacheco, J., Sykes, L., and Scholz, C.: Nature of seismic coupling along simple plate boundaries of the subduction type, *J. Geophys. Res.*, 98, 14133–14160, 1993. 945, 969

Modelling of subduction interplate dynamics

D. Arcay

Title Page

Abstract

Introduction

Conclusions

References

Tables

Figures

◀

▶

◀

▶

Back

Close

Full Screen / Esc

Printer-friendly Version

Interactive Discussion



- Peacock, S. and Hyndman, R.: Hydrous minerals in the mantle wedge and the maximum depth of subduction thrust earthquakes, *Geophys. Res. Lett.*, 26, 2517–2520, 1999. 946
- Peacock, S., Christensen, N., Bostock, M., and Audet, P.: High pore pressures and porosity at 35 km depth in the Cascadia subduction zone, *Geology*, 39, 471–474, 2011. 969
- 5 Ribe, N. and Christensen, U.: Three-dimensional modeling of plume-lithosphere interaction, *J. Geophys. Res.*, 99, 699–682, 1994. 950
- Ruff, L. and Kanamori, H.: Seismic coupling and uncoupling at subduction zones, *Tectonophysics*, 99, 99–117, 1983. 969
- Schmidt, M. and Poli, S.: Experimentally based water budgets for dehydrating slabs and consequences for arc magma generation, *Earth Planet. Sci. Lett.*, 163, 361–379, 1998. 971
- 10 Sobolev, A. and Babeyko, A.: What drives orogeny in the Andes?, *Geology*, 33, 617–620, 2005. 969
- Springer, M.: Interpretation of heat-flow density in the Central Andes, *Tectonophysics*, 306, 377–395, 1999. 971
- 15 Springer, M. and Forster, A.: Heat-flow density across the Central Andean subduction zone, *Tectonophysics*, 291, 123–129, 1998. 971
- Stachnik, J., Abers, G., and Christensen, D.: Seismic attenuation and mantle wedge temperatures in the Alaska subduction zone, *J. Geophys. Res.*, 109, B10304, doi:10.1029/2004JB003018, 2004. 970
- 20 Syracuse, E., van Keken, P. E., and Abers, G.: The global range of subduction zones thermal models, *Phys. Earth Planet. Inter.*, 183, 73–90, 2010. 946
- Tagawa, M., Nakakuki, T., Kameyama, T., and Tajima, F.: The role of history-dependent rheology in plate boundary lubrication for generating one-sided subduction, *Pure Appl. Geophys.*, 164, 125–130, 2007. 969
- 25 Tichelaar, B. and Ruff, L.: Depth of seismic coupling along subduction zones, *J. Geophys. Res.*, 98, 2017–2037, 1993. 968, 969
- Turcotte, D. and Schubert, G.: *Geodynamics: Applications of Continuum Physics to Geological Problems*, John, New York, Cambridge University Press, 1982. 951, 952
- van Hunen, J., van der Berg, A., and Vlaar, N.: On the role of subducting plateaus in the development of shallow flat subduction, *Tectonophysics*, 352, 317–333, 2002. 946
- 30 van Keken, P., King, S., Schmeling, H., Christensen, U., Neumeister, D., and Doin, M.-P.: A comparison of methods for the modeling of thermochemical convection, *J. Geophys. Res.*, 102, 22477–22495, 1997. 949

Modelling of subduction interplate dynamics

D. Arcay

Title Page

Abstract

Introduction

Conclusions

References

Tables

Figures

◀

▶

◀

▶

Back

Close

Full Screen / Esc

Printer-friendly Version

Interactive Discussion



- van Keken, P., Kiefer, B., and Peacock, S.: High-resolution models of subduction zones: implications for mineral dehydration reactions and the transport of water into the deep mantle, *Geochem. Geophys. Geosyst.*, 3, 1056, doi:10.1029/2001GC000256, 2002. 946
- von Herzen, R., Ruppel, C., Molnar, P., Nettles, M., Nagihara, S., and Ekström, G.: A constraint in the shear stress at the Pacific-Australian plate boundary from heat flow and seismicity at the Kermadec forearc, *J. Geophys. Res.*, 106, 6817–6833, 2001. 968
- Wada, I. and Wang, K.: Common depth of slab-mantle decoupling: reconciling diversity and uniformity of subduction zones, *Geochem. Geophys. Geosyst.*, 10, Q10009, doi:10.1029/2009GC002570, 2009. 946, 972
- Wada, I., Wang, K., He, J., and Hyndman, R.: Weakening of the subduction interface and its effects on surface heat flow, slab dehydration, and mantle wedge serpentinization, *J. Geophys. Res.*, 113, B04402, doi:10.1029/2007JB005190, 2008. 946
- Wang, K. and He, J.: Mechanics of low-stress forearcs: Nankai and Cascadia?, *J. Geophys. Res.*, 104, 15191–15205, 1999. 968
- Wang, K. and Suyehiro, K.: How does plate coupling affect crustal stresses in Northeast and Southwest Japan?, *Geophys. Res. Lett.*, 26, 2307–2310, 1999. 968
- Wang, K., Mulder, T., Rogers, G., and Hyndman, R.: Case for very low coupling stress on the Cascadia subduction fault, *J. Geophys. Res.*, 100, 12907–12918, 1995. 968
- Wilks, K. and Carter, N.: Rheology of some continental lower crustal rocks, *Tectonophysics*, 182, 57–77, 1990. 955
- Zhao, D., Hasegawa, A., and Horiuchi, S.: Tomographic imaging of *P*- and *S*-wave velocity structure beneath Northeastern Japan, *J. Geophys. Res.*, 97, 19909–19928, 1992. 970
- Zhao, D., Wang, K., Rogers, G., and Peacock, S.: Tomographic image of low *P* velocity anomalies above slab in northern Cascadia subduction zones, *Earth Planet. Space*, 53, 285–293, 2001. 970
- Zhong, S. and Gurnis, M.: Mantle convection with plates and mobile, faulted plane margins, *Science*, 267, 838–843, 1995. 946
- Ziagos, J., Blackwell, D., and Mooser, F.: Heat flow in Southern Mexico and the thermal effects of subduction, *J. Geophys. Res.*, 90, 5410–5420, 1985. 972

Modelling of subduction interplate dynamics

D. Arcay

Title Page

Abstract

Introduction

Conclusions

References

Tables

Figures

◀

▶

◀

▶

Back

Close

Full Screen / Esc

Printer-friendly Version

Interactive Discussion

**Table 1.** Parameter names and values.

Parameter name	Symbol	Value
Box height	H_0	555 km
Bottom temperature	T_b	1888 K
Surface temperature	T_s	273 K
Mantle density	ρ_m	3300 kg m^{-3}
Mantle radiogenic heat production	A	$9.20 \times 10^{-8} \text{ W m}^{-3}$
Adiabatic gradient	$\left(\frac{\partial T}{\partial z}\right)_{\text{adiab}}$	0.445 K km^{-1}
Thermal diffusivity	κ	$0.8 \times 10^{-6} \text{ m}^2 \text{ s}^{-1}$
Thermal expansion coefficient	α	$3.5 \times 10^{-5} \text{ K}^{-1}$
Heat capacity	c_p	$0.971 \times 10^3 \text{ J K}^{-1} \text{ kg}^{-1}$
Thermal conductivity	k	$2.56 \text{ W m}^{-1} \text{ K}^{-1}$
Dissipation number	$Di = \frac{\alpha g H_0}{c_p}$	0.196
Gravity acceleration	g	9.81 m s^{-2}
Weak layer thickness	H_c	7 km
Cohesive strength	τ_0	1 MPa
Stress exponent in the viscous rheology	n	3
Stress exponent in the brittle rheology	n_p	30
Reference strain rate	$\dot{\epsilon}_{\text{ref}}$	10^{-14} s^{-1}
Yield stress increase with depth (mantle)	γ_m	1.6

Modelling of subduction interplate dynamics

D. Arcay

Table 2. Simulation list.

Simulation	Plate age at trench	Rheology label	Mantle activation energy	Crust activation energy	Activation energy contrast	Activation volume	Viscosity pre-exponential constant	Viscosity at mantle wedge tip	Viscosity jump at box bottom	Crust density stress	Crust yield increase with depth
	A Myr		E_a^m kJ mol^{-1}	E_a^c kJ mol^{-1}	ΔE_a kJ mol^{-1}	V_a $\text{m}^3 \text{mol}^{-1}$	A_0 $\text{MPa}^{-3} \text{s}^{-1}$	v_{asth} Pas	v_{BB}^*	ρ_c kg m^{-3}	γ_c
S6	100	C6	435	370	65	1.5×10^{-5}	19 170.94	2.742×10^{19}	$\times 10$	3120	0.045
S10	100	C10	490	335	155	1.5×10^{-5}	1 467 369.2	2.742×10^{19}	$\times 1$	3120	0.069
S10LG	100	C10LG	490	335	155	1.5×10^{-5}	1 467 369.2	2.742×10^{19}	$\times 1$	3120	0.007
S12	100	C12	435	370	65	1.7×10^{-5}	31 762.4	2.742×10^{19}	$\times 1$	3120	0.045
S13	100	C13	465	360	105	1.7×10^{-5}	339 428.7	2.742×10^{19}	$\times 10$	3120	0.034
S13HG	100	C13HG	465	360	105	1.7×10^{-5}	339 428.7	2.742×10^{19}	$\times 10$	3120	0.061
S13f14	100	C13f14	465	360	105	1.7×10^{-5}	339 428.7	5.235×10^{17}	$\times 10$	3120	0.034
S14	100	C14b	465	360	105	1.7×10^{-5}	339 428.7	2.742×10^{19}	$\times 10$	3120	0.069
S6b	18	C6	435	370	65	1.5×10^{-5}	19 170.94	2.742×10^{19}	$\times 10$	3110	0.045
S10b	18	C10	490	335	155	1.5×10^{-5}	1 467 369.2	2.742×10^{19}	$\times 1$	3300	0.069
S12b	18	C12	435	370	65	1.7×10^{-5}	31 762.4	2.742×10^{19}	$\times 1$	3220	0.045
S12b2	18	C12	435	370	65	1.7×10^{-5}	31 762.4	2.742×10^{19}	$\times 1$	3300	0.045
S13b	18	C13	465	360	105	1.7×10^{-5}	339 428.7	2.742×10^{19}	$\times 10$	3300	0.034
S13b2	30	C13	465	360	105	1.7×10^{-5}	339 428.7	2.742×10^{19}	$\times 10$	3300	0.034
S14b	20	C14b	465	360	105	1.7×10^{-5}	339 428.7	2.742×10^{19}	$\times 10$	3300	0.069

Title Page

Abstract

Introduction

Conclusions

References

Tables

Figures

◀

▶

◀

▶

Back

Close

Full Screen / Esc

Printer-friendly Version

Interactive Discussion



Modelling of subduction interplate dynamics

D. Arcay

a. Depth of interplate kinematic decoupling b. Depth of brittle–ductile transition along the interplate plane

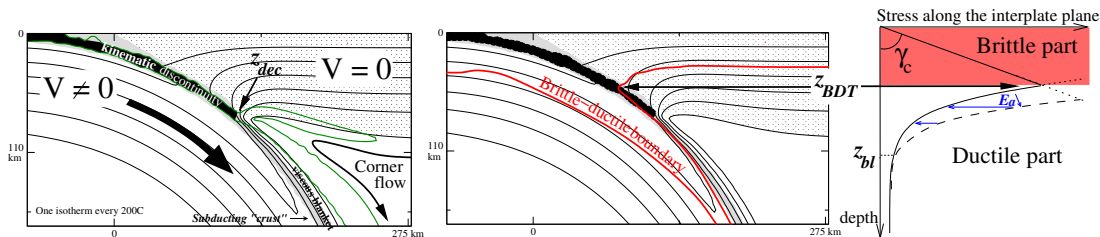


Fig. 1. (a) Definition of the interplate decoupling depth, z_{dec} . Isotherms (black lines) are depicted every 200°C . An outline of high strain strain is schematically represented by the thick green line. The light-dotted domain highlights the motionless upper lithosphere. The subduction interplate plane, here envisioned as a kinematic discontinuity, is colored in black. The subducting weak layer, located at the subducting lithosphere surface as an oceanic subducting crust layer, is depicted in light grey. The “viscous blanket” refers to the thermal boundary layer formed by asthenospheric cooling at the subducting lithosphere surface (Kincaid and Sacks, 1997). (b) Definition of the brittle-ductile transition depth, z_{BDT} . The brittle-ductile boundary (thick red line) connects rock elements where the pseudo-brittle strength, ν_b , equals the non-Newtonian viscosity, ν_v . The medium is thus modelled as brittle above the red line and ductile below, as sketch in the stress-depth diagram along the interplate plane the on the right. An energy activation decrease if asthenosphere viscosity is unchanged at the upper lithosphere depth, z_{bl} , is sketched in blue to highlight its effect on z_{BDT} shallowing.

Discussion Paper | Discussion Paper | Discussion Paper | Discussion Paper | Discussion Paper

Title Page

Abstract

Introduction

Conclusions

References

Tables

Figures

◀

▶

◀

▶

Back

Close

Full Screen / Esc

Printer-friendly Version

Interactive Discussion



Modelling of
subduction interplate
dynamics

D. Arcay

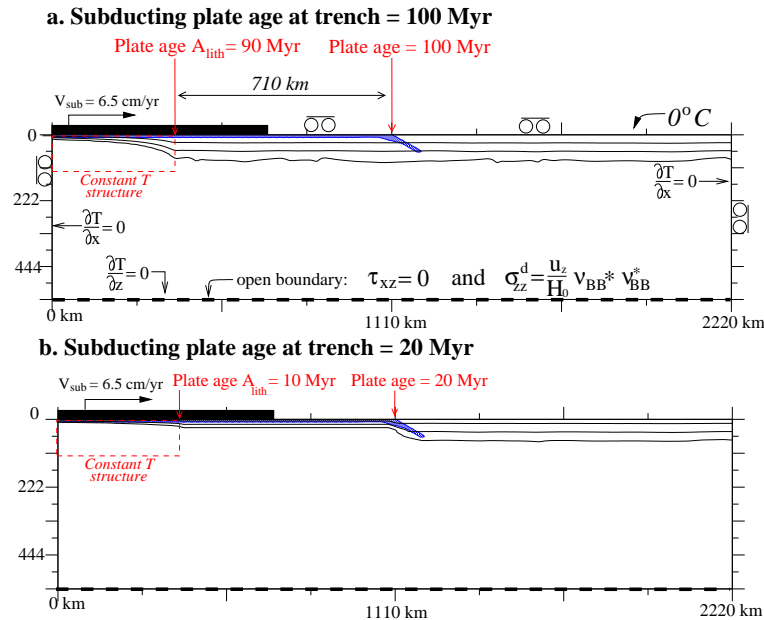


Fig. 2. Boundary conditions for both old and young subducting lithospheres and thermal conditions when subduction is initiated. The weak layer geometry imposed at simulation start is highlighted in blue. The subducting lithosphere velocity, v_{sub} , is imposed on the plate in a 832 km wide and 16 km deep domain, respectively, counted from the box left-hand side and from the box surface, respectively. Slip is free on the surface remaining at the top, which allows the subduction geometry for evolving freely. Isotherms are depicted every 400 °C. The temperature field constantly maintained in the red dashed area, to mimic the lithosphere cooling from formation at the ridge (top left corner) to a chosen lithosphere age, A_{lith} , 400 km far away (right boundary of the red-dashed box). **(a)** Model boundary and initial conditions for a converging lithosphere 100 Myr-old at the trench. A_{lith} is set to 90 Myr. **(b)** Boundary and initial conditions for a converging lithosphere ~ 20 Myr old at the trench. A_{lith} is set to 10 Myr.

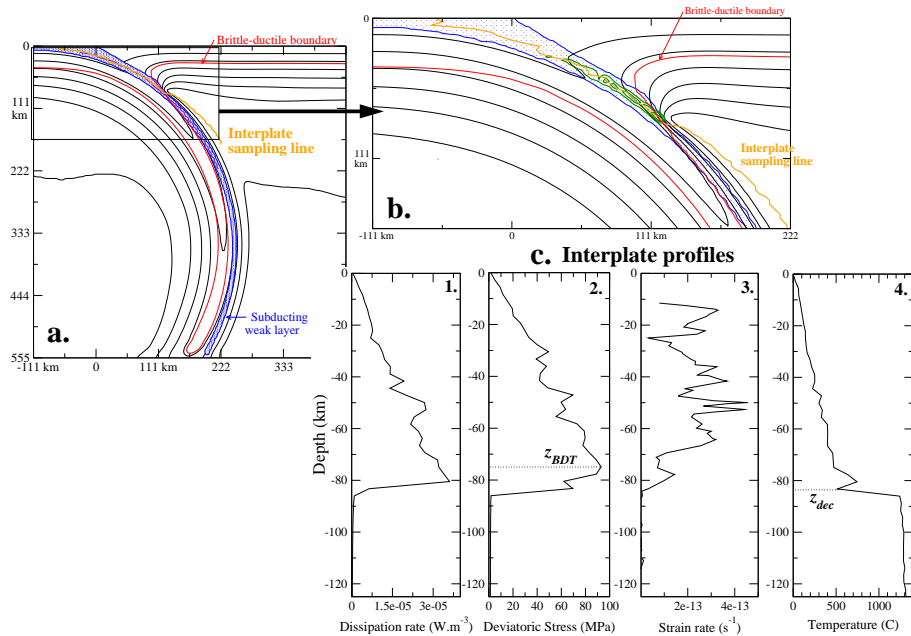


Fig. 3. (a) Simulation S13 (rheology C13, 100 Myr year-old lithosphere at trench, Table 2), 16 Myr after subduction initiation. The trench is located at the abscissa $x = 0$ km. One isotherm (black lines) every 200°C . The interplate sampling line (orange line) is defined by locations of maximum dissipation energy rates (see the text for details). Along the labelled “brittle-ductile boundary” (thick red line), the pseudo-brittle strength, v_b , equals the non-Newtonian viscosity, v_v . (b) Close-up on the subduction interface. Outlines of dissipation energy rate (green lines) are depicted every $10 \mu\text{Wm}^{-3}$. (c) Profiles interpolated along the interplate sampling line, from left to right, (1) dissipation energy rate, (2) second invariant of the deviatoric stress tensor, (3) second invariant of the strain rate tensor, and (4) temperature. Note that in this particular case, the brittle-ductile transition depth, z_{BDT} , is so close to the interplate decoupling depth, z_{dec} , that they are assumed to be roughly equal.

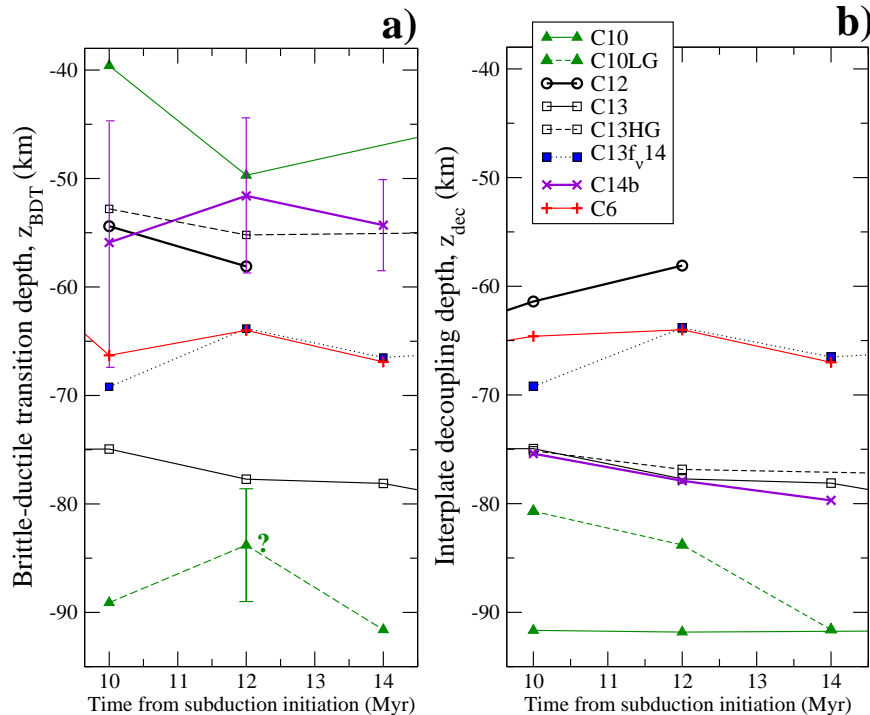


Fig. 4. Brittle-ductile transition depth simulated as a function of time elapsed from subduction initiation, for an old subducting lithosphere (simulations S6, S10, S10LG, S12, S13, S13HG, S13f14, and S14 in Table 2). The question mark underlines the assumed estimate for z_{BDT} at 12 Myr for rheology C10LG, with an extreme friction coefficient for the weak layer, which makes the measurement impossible at that time. A minimum and maximum values can nevertheless be measured, as illustrated by the uncertainty bar. The assumed z_{BDT} value at 12 Myr is set to the middle depth in the uncertainty interval, as it also corresponds to the interplate decoupling depth at this time (b). It is indeed likely that $z_{BDT} = z_{dec}$ in this case. (b) Interplate decoupling depth evolution, for an old subducting lithosphere, simulated in the same models as in (a).

**Modelling of
subduction interplate
dynamics**

D. Arcay

Title Page

Abstract

Introduction

Conclusions

References

Tables

Figures

◀

▶

◀

▶

Back

Close

Full Screen / Esc

Printer-friendly Version

Interactive Discussion

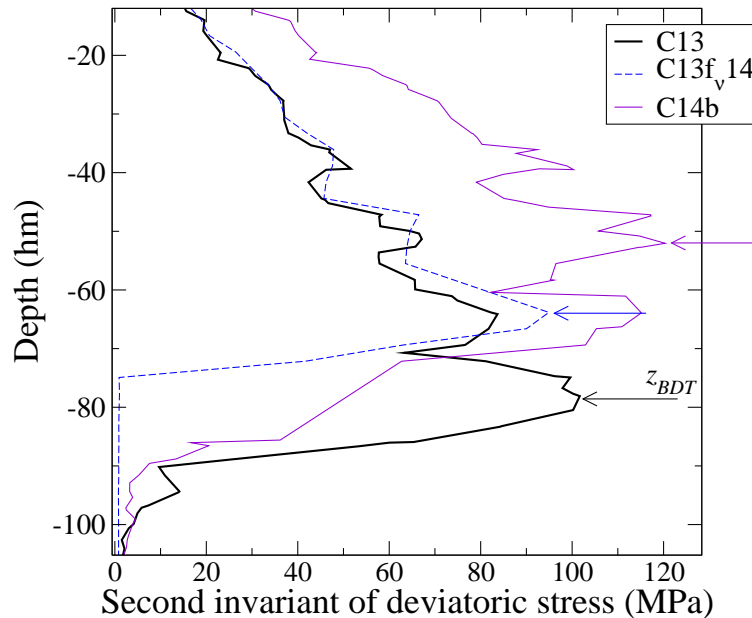


Fig. 5. Stress profiles computed along the subduction interface for an old incoming lithosphere, 12 Myr after subduction initiation, for simulations S13, S13f14, and S14 (Table 2). Estimates of the brittle-ductile transition depth are underlined by thin arrows.

**Modelling of
subduction interplate
dynamics**

D. Arcay

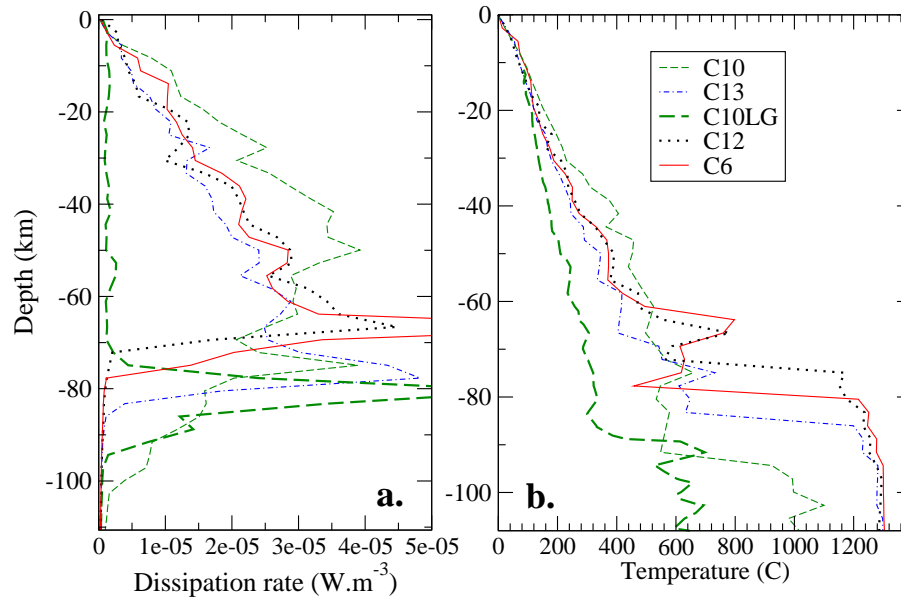


Fig. 6. (a) Interplate profiles of dissipation rates simulated 12 Myr after simulation initiation in models S6, S10, S12, S13, and S10LG. (b) Corresponding geotherms simulated at the same time.

Title Page

Abstract

Introduction

Conclusions

References

Tables

Figures

◀

▶

◀

▶

Back

Close

Full Screen / Esc

Printer-friendly Version

Interactive Discussion



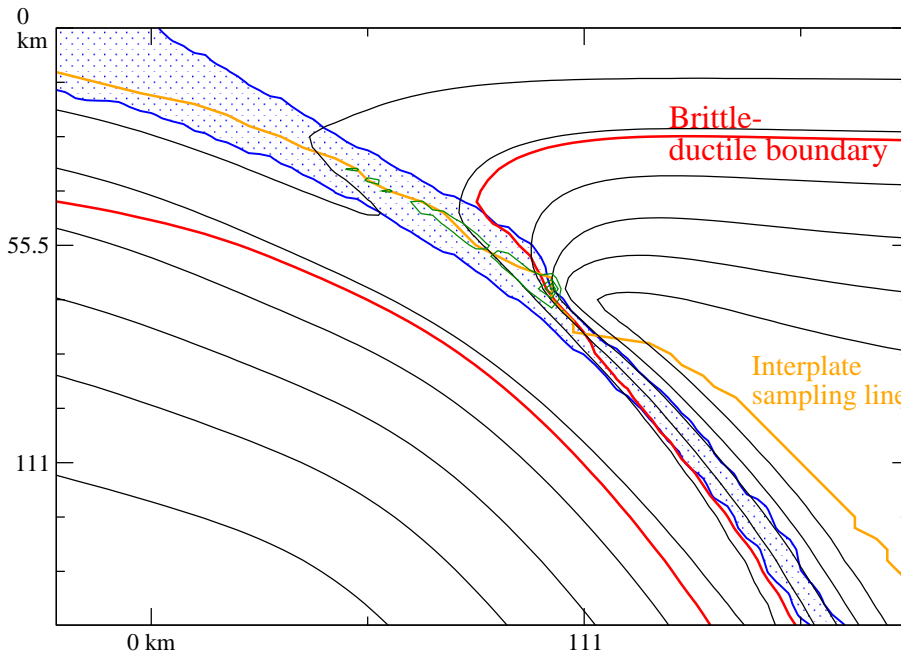


Fig. 7. Simulation S6 (rheology C6, 100 Myr year-old lithosphere at trench, Table 2), 12 Myr after subduction initiation, close-up on the subduction interface. One isotherm (black lines) every 200 °C. The interplate sampling line (orange line) is defined by locations of maximum dissipation energy rates. Along the labelled “brittle-ductile boundary” (thick red line), the pseudo-brittle strength, ν_b , equals the non-Newtonian viscosity, ν_v . The blue filled domain represents the weak subducting layer. Outlines of dissipation energy rate (green lines) are depicted every $20 \mu\text{W m}^{-3}$.

Modelling of subduction interplate dynamics

D. Arcay

Title Page

Abstract Introduction

Conclusions References

Tables Figures

◀ ▶

◀ ▶

Back Close

Full Screen / Esc

Printer-friendly Version

Interactive Discussion



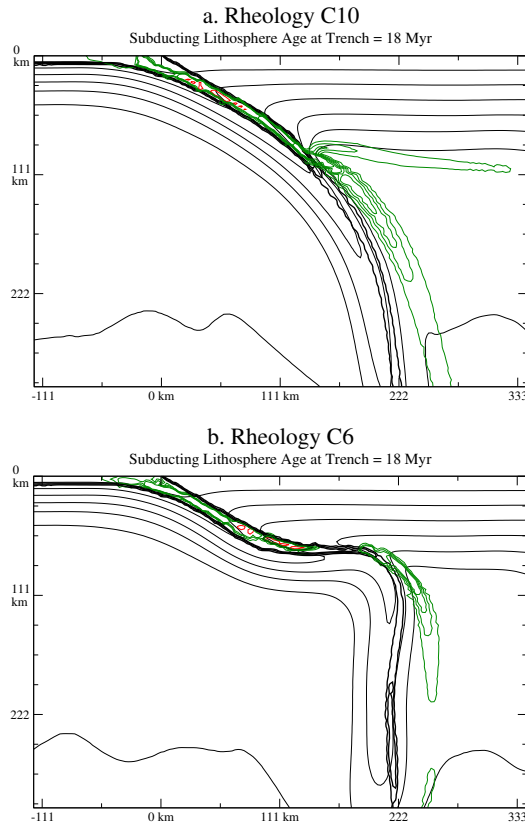


Fig. 8. Simulation of a young and hot lithosphere subduction, for rheology C10 (**a**, simulation S10b, Table 2) and C6 (**b**, simulation S6b), 6 Myr after convergence initiation. Close-up on the subduction zone. One isotherm (black lines) every 200 °C. Thick black outlines are depicted every 20 % increase in crust concentration. Outlines of dissipation energy rate (red lines) are depicted every 20 μWm^{-3} . Outlines of constant strain rates (green lines) are depicted every $4 \times 10^{-14} \text{ s}^{-1}$.

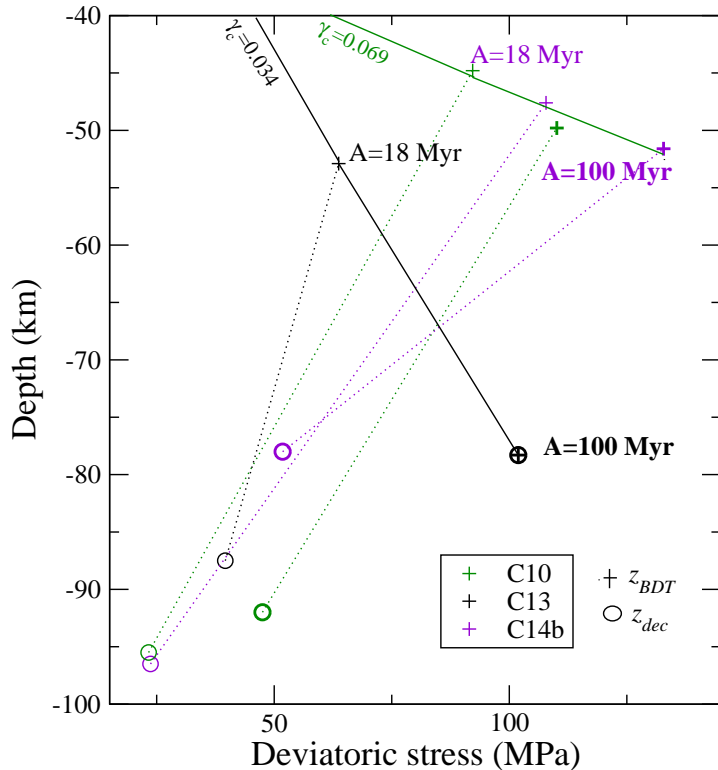


Fig. 9. Deviatoric stress (second invariant) versus depth modeled at the BDT depth, z_{BDT} (crosses), and at the interplate down-dip extent, z_{dec} (empty circles), 12 Myr after subduction initiation, for a ~ 18 Myr old subducting lithosphere (thin symbols) and a 100 km thick plate (thick symbols). Simulations performed with rheology C10 (green color, Table 2), C13 (black color), and C14b (violet color). Solid lines sketch brittle yield stress increasing with strength, whereas dotted lines symbolically represent the stress drop in the lower part of the interplate plane.

Modelling of subduction interplate dynamics

D. Arcay

Title Page

Abstract

Introduction

Conclusions

References

Tables

Figures

◀

▶

◀

▶

Back

Close

Full Screen / Esc

Printer-friendly Version

Interactive Discussion



Modelling of subduction interplate dynamics

D. Arcay

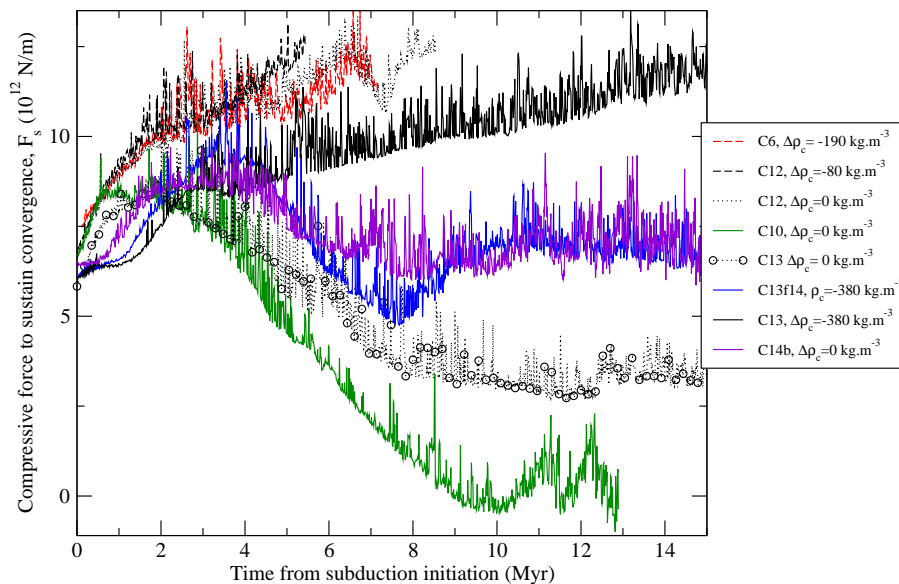


Fig. 10. Compressive force through time, applied on the young subducting plate, to sustain a constant convergence rate of 6.5 cm yr^{-1} , as a function of rheological model and weak layer density.

Title Page

Abstract

Introduction

Conclusions

References

Tables

Figures

◀

▶

◀

▶

Back

Close

Full Screen / Esc

Printer-friendly Version

Interactive Discussion

